CURVELET TRANSFORM-BASED TECHNIQUES

FOR

BIOMETRIC PERSON IDENTIFICATION

Vijaya Kumar Emani

A Thesis

in

The Department

of

Electrical and Computer Engineering

Presented in Partial Fulfillment of the Requirements

for the Degree of Master of Applied Science (Electrical and Computer Engineering) at

Concordia University

Montreal, Quebec, Canada

December 2010

CONCORDIA UNIVERSITY
School of Graduate Studies

This is to certify that the thesis prepared

By: **Vijaya Kumar Emani**

Entitled: **Curvelet Transform-Based Techniques for Biometric Person Identification**

and submitted in partial fulfillment of the requirements for the degree of

Master of Applied Science (Electrical and Computer Engineering)

complies with the regulations of the University and meets the accepted standards with respect to originality and quality.

Signed by the final examining committee:

_____ Chair
Dr. Dongyu Qiu

_____ External to Program
Dr. Amr Youssef

_____ Examiner
Dr. M.N.S. Swamy

_____ Examiner
Dr. W.P. Zhu

_____ Supervisor
Dr. M.O. Ahmad

Approved by _____
Dr. M. Kahrizi, Graduate Program Director

Nov. 26, 2010 _____
Dr. Robin A.L. Drew, Dean
Faculty of Engineering and Computer Science

ABSTRACT

Curvelet Transform-Based Techniques for Biometric Person Identification

Vijaya Kumar Emani

Biometric person identification refers to the recognition of a person based on the physical or behavioral traits. Palm print based biometric identification system is one of the low cost biometric systems, since the palm image can be obtained using low cost sensors, such as desktop scanners and web cameras. Because of ease of image acquisition of palm prints and identification accuracy, palm images are used in both uni-modal and multimodal biometric systems. A multi-scale and multi-directional representation is desirable to represent thick and scattered thin lines of a palm image. Multi-scale and multi-directional representation can also be used in image fusion, where two images of two different biometric traits can be fused to a single image to improve the identification accuracy. Face and palm images can be fused to keep the desired high pass information of the palm images and the low pass information of the face images. The Curvelet transform is a multi-scale and multi-directional geometric transform that provides a better representation of the objects with edges and requires a small number of curvelet coefficients to represent the curves.

In this thesis, two methods using the very desirable characteristics of the curvelet transform are proposed for both the uni-modal and bi-modal biometric systems. A palm curvelet code (PCC) for palm print based uni-modal biometric systems and a pixel-level fusion method for face and palm based bi-modal biometric systems are developed. A simple binary coding technique that represents the structural information in curvelet

directional sub-bands is used to obtain the PCC. Performance of the PCC is evaluated for both identification and verification modes of a palm print based biometric system, and then, the use of PCC in hierarchical identification is investigated. In the pixel-level fusion scheme for a bi-modal system, face and palm images are fused in the curvelet transform domain using *mean-mean fusion* rule. Extensive experimentations are carried out on three publicly available palm databases and one face database to evaluate the performance in terms of the commonly used metrics, and it is shown that the proposed methods provide a better performance compared to other existing methods.

ACKNOWLEDGEMENTS

I would like to express my deep gratitude to my supervisor Professor M. Omair Ahmad for his constant support and encouragement during the span of this research. I am thankful to my parents and brothers who supported me morally and finically. Finally, I would like to thank my friends and colleagues for their support and encouragement.

CONTENTS

List of Tables

List of Figures

List of Acronyms

CDSC	:	Curvelet Directional Subband Code
CIR	:	Correct Identification Rate
EER	:	Equal Error Rate
FAR	:	False Acceptance Rate
FFT	:	Fast Fourier Transform
FIR	:	False Identification Rate
FRR	:	False Rejection Rate
GAR	:	Genuine Acceptance Rate
GPDS	:	grupo de procesado digital de senales
IITD	:	Indian Institute of Technology, Delhi
PCA	:	Principal Component Analysis
PCC	:	Palm Curvelet Code
PolyU	:	Poly Technique University
ROC	:	Receiver Operating Characteristics
ROI	:	Region of Interest

List of Symbols

β	:	Number of blocks in a directional sub band
δ	:	Downsample ratio for a directional sub band
κ	:	Percentage of significant coefficients in a directional sub band
N_{AI}	:	Total number of accepted imposters
N_G	:	Total number of genuine claims
N_I	:	Total number of imposter claims
N_{QS}	:	Total number of query samples
N_{RG}	:	Total number of rejected genuine claims
N_{WI}	:	Total number of wrongly identified samples
N_{WR}	:	Total number of wrongly rejected samples
$c^D(j,l,k)$	:	Discrete curvelet coefficient at scale j, direction l, and position k
$\varphi^D_{j,l,k}$	:	Digital curvelet waveform at scale j, direction l, and position k
$V_j(\omega)$	:	Angular window in polar coordinates at scale j
$\widetilde{W_j}(\omega)$	:	Radial window in polar coordinates at scale j
$\widetilde{U_{j,l}}(\omega)$	:	Curvelet in frequency domain
Φ	:	Low pass one dimensional windows
ψ	:	Average image in PCA
χ	:	Difference image from the training space in PCA
S	:	Euclidean distance

N_{TS}	:	Number of training samples
N_{SC}	:	Number of samples in each class
N_{TE}	:	Total number of experiments
N_{PCA}	:	Number of principal components

Chapter 1

Introduction

Person identification is a process of recognizing the identity of a person based on a claimed identity, such as physical key, password, and identity card. Automatic person identification has an important role in everyday life, for example, students use personal identification numbers (PIN) to login a shared computer and employees use identity cards for attendance at work place. Traditional identification methods are based on possession of an identity like access card or knowledge of a secret number. Traditional identification methods check only the possession of a piece of identity or the knowledge of a secret number, but not the right ownership. Moreover access cards can be stolen and the PIN numbers can be guessed. Anyone having the access card or PIN number will be authorized. So an identification process based on "who he/she is" is more secured than traditional methods which are based on "what he/she has" or "what he/she knows" [41]. Biometric identification comes under the category in which a person is identified based on "who he/she is".

Biometric identification is a process of recognizing people based on his/her physical or behavioral traits. Iris, face, fingerprint, palmprint and hand geometry are popular

examples of physical traits. Behavioral traits include speech, gait and signature. Biometric identification is more reliable and secured compared to automatic traditional identification. In biometric identification, a sensor acquires the physical or behavioral trait, and features are extracted from the pre processed signal, these features are compared with a template database to identify the person. Low cost sensors, hardware, efficiency, and fast algorithms made biometrics to spread in all levels of security systems, starting from attendance, door locks and to a high level security like border crossing.

1.1 Motivation

Even though great deal of research has been conducted on different biometric traits like face, iris, fingerprint and palmprint, each biometric trait has its own advantages and disadvantages in terms of ease of accessibility, uniqueness, and cost of the sensors. For example face image acquisition is simple and cost effective compared to iris scanning, because a simple web camera can be used to acquire a face image and the person to be identified need not pay special attention during image acquisition. Palmprint belongs to one of those physiological traits which can be acquired using a low cost camera or scanner. Many researchers have shown that the performance of palmprint based biometric systems is comparable to those of face, fingerprint and hand geometry. The information in palmprint images is in the form of thick, regular and thin irregular curves called principal lines and wrinkles, respectively. Most of the feature extraction

algorithms aim at representing this information of curves effectively. These methods can be broadly classified into statistical methods, line-based methods, subspace-based methods, and coding methods [2].

In statistical approach various statistical measurements are obtained either directly from the preprocessed palm images or from the transformed versions. In the transform domain, Fourier transform [1] and wavelet transform [4] are used to extract the statistical features. In [4], authors have used wavelet transform and directional context modeling to represent the edge like features of a palm image. Statistical features, such as density, center of gravity, and energy are computed to represent a given palm image. This method is verified on a small size database of 200 palms. In [1], Fourier transform of the image is obtained and the Fourier plane is divided into concentric circles and directional wedges. The energy of the concentric circles and directional wedges are used as a feature vector. Neither the Fourier transform nor the wavelet transform can represent the directional features accurately.

There are some other transforms that can represent the directional features, such as dual tree complex wavelet transform [6], contourlet transform [7], and curvelet transform [8]. In [6], support vector machine is used as classifier to train the directional feature vectors. In [7], contourlet transform and the Fourier transform features are used to represent the given palm images. Palm image is decomposed into a preset number of scales and directions using contourlet transform. Magnitude of the Fourier transform of each contourlet subband is used as a feature vector. Adaboost [38] is used

to train these feature vectors. Even though the size of the feature vector has not been mentioned in the method explicitly, the size of the input palm image and the algorithm suggests high dimensionality. Moreover this method requires training. In [8], first generation digital curvelet transform is used; the magnitude and positions of the significant coefficients are used as a feature vector. In [9], complex wavelet transform is used to match two palm images. A modified structural similarity index is applied to match the images in complex wavelet domain. The main drawback of this method is the very high dimensionality of feature vectors. Even though all these methods used the transforms that can represent the directional features, none of these methods used the directional structure information explicitly.

Line based methods extract line like features from the palmprint. In [11], line edge map of the palm images are obtained and line segment Hausdorff distance is used as a classifier. The method was tested on a small database of size 200 palms, and the authors have claimed identification rate of 96 %. In [12], Sobel and morphological operators have been applied to extract features. A neural network is then used to train the features. In subspace methods, principal component analysis (PCA), Fisher linear discriminant analysis (FLDA), and independent component analysis (ICA) have been applied either directly on the palmprint image [1] or on feature vectors [10] to reduce the dimensionality. Subspace based methods require training. Every time a new template is added, training process has to be repeated.

In [5] Gabor filters have been used to extract the texture feature. A coding scheme similar to Iris code is applied. Even though good error rates are claimed, feature matching is based on translations. Each feature is translated vertically and horizontally before matching. This is acceptable in verification process, but consumes more time in identification process, especially in large databases.

Because of the low resolution images and ease of image capturing, palmprint features have been used in multimodal biometric systems to improve the performance and to overcome the limitations of the other biometric traits. The fusion of the information from different biometric traits has been conducted at various levels of a biometric identification process, such as sensor level, feature level, and classifier level. When two biometric traits such as face and palm are obtained from the same imaging setup, fusion can be done at pixel level. In [26], Gabor transform have been used in fusion process. Gabor transform is obtained for 4 scales and 8 orientations. The transformed images of face and palm are simply concatenated to obtain fused image. A kernel discriminative common vectors algorithm with radial basis function (RBF) network is used in feature extraction and classification. In [27], the wavelet transform domain fusion have been applied and scale invariant feature transform (SIFT) have been used in feature extraction. In [26], images are concatenated in the transform domain. Thus this process cannot be considered as fusion of features. In [27], fusion is applied in wavelet transform domain. Effective fusion can be achieved if more directional bandpass images are included.

Curvelet transform is a multi-scale and multi-directional transform developed by Cand`es et al. [13], to overcome the limitations of the conventional 2-D discrete wavelet transform [14]. Curvelet transform provides almost optimal representation of objects with curve singularities. That means, curvelet transform needs relatively a small number of coefficients to represent a line or a curve in a given image. Two factors encourage the usage of curvelet transform for palmprints. One is the optimal representation of edges and the second factor is multi-scale and multi-directional representation.

Main features in palm images are principal lines and wrinkles. Principal lines are regular and thick structure, whereas wrinkles are irregular and thin structure. Wrinkles are scattered in different orientations. Multi-scale and multi-directional representation gives a better representation of these scattered wrinkles. This representation also helps in improving the fusion scheme in pixel-level fusion of face and palm. Since the lines and curves are represented by only a small number of coefficients of curvelet transform, we expect low dimensionality feature vector.

A major problem in palmprint identification systems is the size of the database. To scan a large database, we need to adapt to a guided search to improve the speed of the identification process. Multiple methods are needed to extract multiple features for a guided search. Instead of using multiple methods to extract multiple features, it is desirable to extract multi-scale features using one technique to develop a guided search. Since curvelet transform is multi-scale and multi-directional decomposition, features at various scales and directions can be used in guided search.

Since the curvelet transform has the very characteristics desired by the biometric applications, it would be worth investigating the use of curvelet transform.

1.2 Problem Statement

Palmprint-based biometric systems have gained more interest because of their ease of data acquisition and uniqueness. In low resolution palm images the features are mainly principal line features and wrinkle features. Principal line features are regular and thick lines, wrinkles are thin, irregular features and wrinkle features can be classified into coarse wrinkles and fine wrinkles [1]. These features have to be accurately measured in terms of their structure for a better palmprint identification system. Because of orientation information and coarse and fine scale structure, an efficient feature extraction is required to measure these features. A multi-scale and multi-directional representation of the palmprint is necessary.

One of the advantages of palmprint is its application in bi-modal or multimodal biometric systems. In multimodal systems different modalities are fused to improve the accuracy and security. This fusion is carried out at different levels of identification process, for example, at sensor level, at feature level, and at classifier level. A pixel-level fusion of face and palm is advantageous because one feature extraction technique and one classifier are sufficient for the system.

The objective of this thesis is to propose curvelet transform-based techniques for palmprint based uni-modal biometric system, and face- and palm-based bi-modal

biometric system. A curvelet transform-based coding technique is proposed to represent the line and curve features of a palmprint. A guided search scheme is also proposed using this technique. Extensive experimentations are conducted on three different palmprint databases to evaluate the performance of the proposed method. Finally a pixel-level fusion scheme in curvelet transform domain for face and palmprint based bi-modal biometric system is proposed.

1.3 Organization of the Thesis

This thesis is organized into three parts, overview of relevant concepts, proposed methods for uni-modal and bi-modal biometric systems, experiments and analysis.

In Chapter 2, an overview of the relevant concepts is given. Modes of operations of a biometric system, the parameters used in performance evaluation of a biometric system, curvelet transform and different databases used in this thesis are explained. Various errors rates used in a performance evaluation, such as false acceptance rate (FAR), and false rejection rate (FRR) and their effects are detailed. Basic concepts of curvelet transform and its implementation details are explained. Details of the research conducted on palmprint recognition using curvelet transform are also given. Finally various databases used in this thesis are discussed. Size of the databases and image acquisition procedures are explained.

In Chapter 3, curvelet transform based techniques for the uni-modal and bi-modal biometric systems are proposed. The details of the coding approach to extract the

directional line features of a given palmprint and the details of the distance metrics are explained. A pixel-level fusion scheme of face and palm for a bi-modal biometric system is detailed.

In Chapter 4, details of the experiments and the results are presented for both uni-modal and bi-modal biometric systems. The experimental setup detailing the training databases, test databases and various parameters is explained followed by the results and comparisons.

Concluding remarks and the scope for the future research are detailed on Chapter 5.

Chapter 2

Overview of Relevant Topics

In this chapter, some concepts relevant to this thesis are presented. Details of the palmprint characteristics and preprocessing methods to extract the region of interest (ROI) are explained. Different modes of a biometric system and the metrics used in the performance evaluation are detailed followed by the details of curvelet transform. Finally various databases used in this thesis are explained.

2.1 Characteristics of Palmprint

"A palmprint is defined as the skin patterns of a palm, composed of the physical characteristics of the skin patterns such as lines, points, and texture"[1]. Epidermis, the outermost layer of the skin, finger movements and the tissue structure determine the line features of the palm [1]. These line features on the palm can be classified into three main categories, principal lines, wrinkles and ridges. Principal lines are the regular and the thickest lines of the palm. Wrinkles are the irregular and thin lines. Fingerprint-like lines of the palm are the ridges. The ridges in the fingerprint and palm are due to the thickening of the epidermis [1]. An example hand image is shown in Fig. 2.1. Principal lines and wrinkles can be observed in low resolution palm images, whereas ridges can

be seen only in high resolution palm images. For an online palm identification system, images of 75 dpi / 150 dpi resolution are sufficient [1].

2.2 Palm Preprocessing

Palm preprocessing refers to the extraction of ROI and enhancement of the ROI. Entire palm region is not necessary to extract line features, only the center region that covers the maximum possible length of the principal lines is sufficient. Palmprint alignment is also important to minimize the system errors. So ROI extraction and enhancement are carried out in preprocessing stage. There have been many methods proposed in the literature to align and extract the center part of the palm region [1], [22]. For the alignment of the palm image, one needs to find the orientation of the palm image.

There are two methods in the literature to find the orientation, one is based on ellipse fitting [2], in this method an ellipse that fits the boundary of the given hand image is obtained. The orientation of hand image is obtained by the major axis of the ellipse. The second method is based on the extraction of key points [1]. These key points help in deciding the coordinate system. Usually, the key points are the valley points between index finger and middle finger, and between ring finger and the little finger. The line joining these two points gives the orientation information. In ROI extraction, the center of the palm region is obtained and a fixed size of palmprint is cropped around the center point. The crop area can be obtained by the key points. Using key points, the coordinate system of the palm region is fixed and the ROI is cropped with reference to the coordinate system.

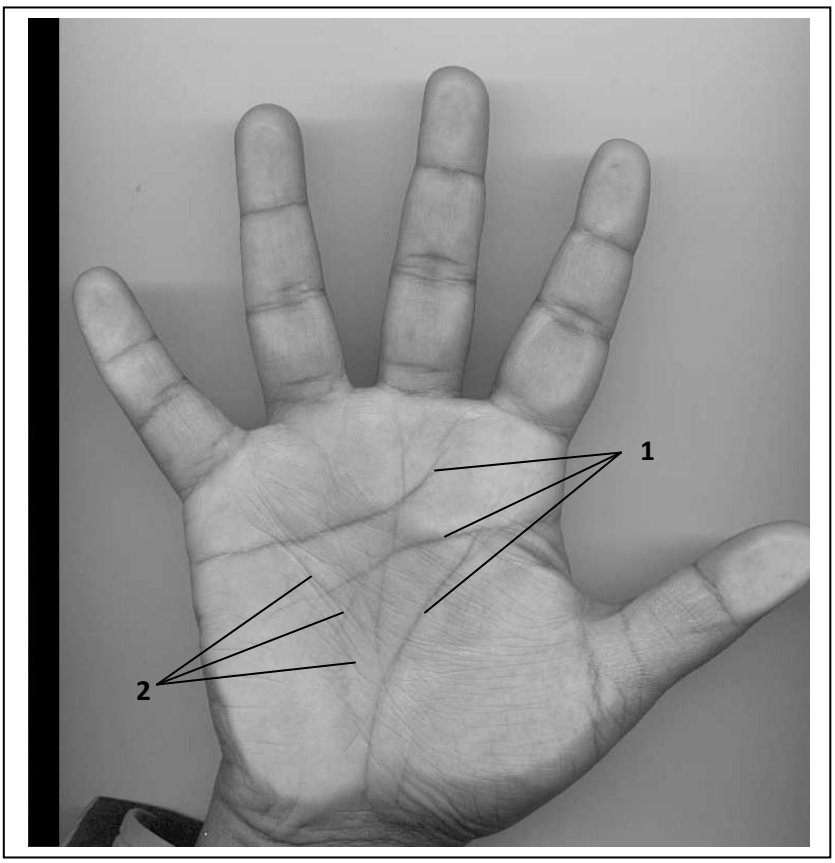

Figure 2.1: Hand image scanned using a desktop scanner, showing principal lines (1) and wrinkles (2).

In some other methods the center point has been obtained using morphological operations [22]. Image erosion is carried out with a square type structuring element to find a square that best fits in. Distance transform also have been used to find the center of the palm region [23]. In this work, author used key point based palm alignment and ROI extraction. The main steps in preprocessing can be summarized as follows.

a. Apply a low pass Gaussian filter to smooth the palm image.

b. Apply a proper threshold to binarize the palm image.

c. Apply morphological operations like hole filling.

d. Trace the boundary of the palm image to fix the key points.

e. Find the orientation of the palm image.

f. Fix the coordinate system to crop the region of interest.

A smoothed hand image and its binary image are shown in Fig. 2.2. It is clear from Fig. 2.2(b) that a proper uniform background helps in effective threhsolding. The process of key point detection and alignment are shown in Fig. 2.3. Finally image enhancement is applied to enhance the line features. Contrast limited adaptive histogram equalization is a good choice to enhance the line features.

2.3 Modes of Biometric System and Metrics used for Performance Evaluation

A biometric system can be operated in two modes, identification mode and verification mode. In identification mode, the person has to be identified based on the biometric feature without any prior information. Identification is a one-many matching process.

A query biometric feature is compared with stored templates to obtain a set of matching scores. If the scores are less than a prefixed threshold, a classifier identifies the query sample to a best match in the registration database. In verification, the query biometric sample is matched against one template that is claimed by an additional identity card of the person to be verified. Verification process is a one-one matching process. In identification mode, correct recognition rate (CRR) or correct identification rate (CIR), false rejection rate (FRR) and false identification rate (FIR) are the important parameters. CIR, FIR and FRR are defined as follows

(a)

(b)

Figure 2.2: (a) A sample hand image (b) Binary image after a fixed thresholding.

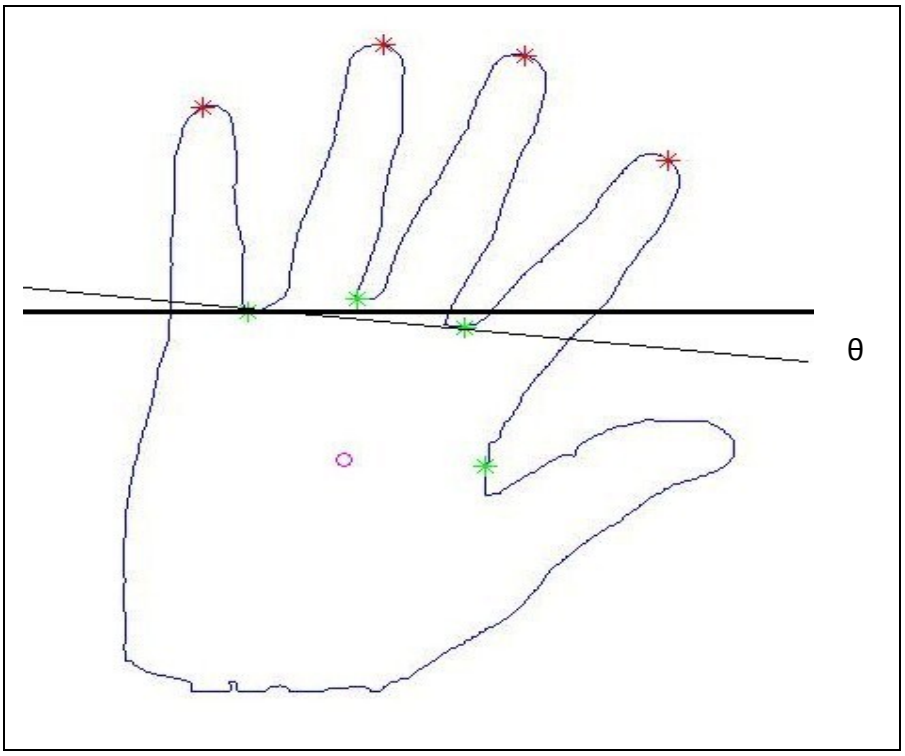

Figure 2.3: Boundary of a hand image showing key points and the angle of rotation θ

$$CIR = \frac{N_{CI}}{N_{QS}} \times 100$$

$$FIR = \frac{N_{WI}}{N_{QS}} \times 100$$

$$FRR = \frac{N_{WR}}{N_{QS}} \times 100$$

where N_{QS} is the total number of query samples, N_{WI} is the total number of wrongly identified samples and N_{WR} is the total number of wrongly rejected samples. The effect of the threshold on CIR, FIR and FRR is also an important measurement in identification process.

In verification mode, false acceptance rate (FAR), false rejection rate (FRR), and equal error rates (EER) are important performance evaluation parameters. These parameters can be obtained by calculating the genuine and impostor score distributions and are defined as follows,

$$FAR = \frac{N_{AI}}{N_I} \times 100$$

$$FRR = \frac{N_{RG}}{N_G} \times 100$$

where N_{AI} is the total number of accepted imposters, N_I is the total number of imposter claims, N_{RG} is the total number of rejected genuine claims, and N_G is the total number of genuine claims. EER is the rate at which FAR is equal to FRR. FAR and FRR are useful parameters in comparing two biometric systems. At a given threshold, a biometric system that gives low FAR and low FRR is a better one. The usage of a biometric system at different security levels depends on FAR and FRR. For example, in a high level security system very low FAR is desirable, whereas in low level security system low FRR is desirable. The effect of the threshold on FAR and FRR can be observed using receiver operating characteristics (ROC). ROC is the plot between genuine acceptance rate (GAR) and false acceptance rate (FAR). Genuine acceptance rate is defined as $GAR = 100 - FRR$. Fig. 2.4 shows a plot of genuine and impostor distributions. A threshold T is selected to get minimum FAR and minimum FRR. The area under the genuine distribution for above threshold T gives the FRR and the area under the imposter distribution and below threshold T gives the FAR.

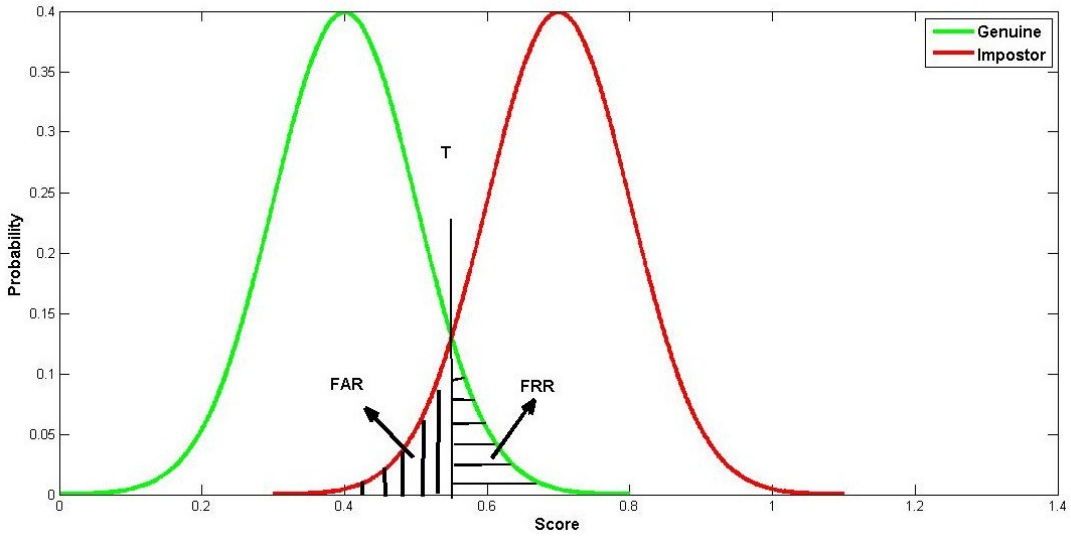

Figure 2.4: Calculation of FAR and FRR at a given threshold T.

2.4 Curvelet Transform

Curvelet transform (CT) is a geometric transform developed by Emmanuel Cand`es et al. [13] to overcome the inherent limitations of wavelet like transforms. Curvelet transform is a multi-scale and multi-directional transform with needle shaped basis functions. Basis functions of wavelet transform are isotropic and thus it requires large number of coefficients to represent the curve singularities. Curvelet transform basis functions are needle shaped and have high directional sensitivity and anisotropy. Curvelets obey parabolic scaling. Because of these properties, curvelet transform allows almost optimal sparse representation of curve singularities [13]. The curvelet transform at different scales and directions span the entire frequency space, which is not the case with other directional transforms such as Gabor wavelets.

Curvelet transform has undergone a major revision since its invention [13]. The first generation curvelet transform is based on the concepts of ridgelet transform [13]. The

curve singularities have been handled by smooth partitioning of the bandpass images. In each smooth partitioned block the curve singularities can be approximated to a line singularity. A ridgelet transform is applied on these small blocks, where ridgelets can deal the line singularities effectively. To avoid blocking artifacts, the smooth partitioning is done on overlapping blocks which results in redundancy, and the whole process involves subband decomposition using atrous wavelet transform, smooth partitioning and ridgelet analysis on each block; this process consumes more time. The implementation of second generation curvelet transform is based on the Fourier transform and is faster, less complex, and less redundant [13].

Two implementations have been proposed in second generation curvelet transform, one is based on un-equispaced fast Fourier transform (USFFT) and the second one is based on wrapping technique [13]. Wrapping based method is simple and easy to understand.

The frequency tiling by the discrete curvelet transform is shown in Fig. 2.5. We can observe that the entire frequency plane is covered by the curvelets at different scales and orientations. Fig. 2.6 shows some curvelets at different scales and orientations in both spatial and frequency domain. As the scale is increased, the curvelets are more sensitive to the orientation. This can be observed in this figure. The curvelet in spatial domain at scale 4 is smaller and finer to the one at scale 3 and it can be observed that curvelets show oscillating behavior perpendicular to the orientation in the frequency domain.

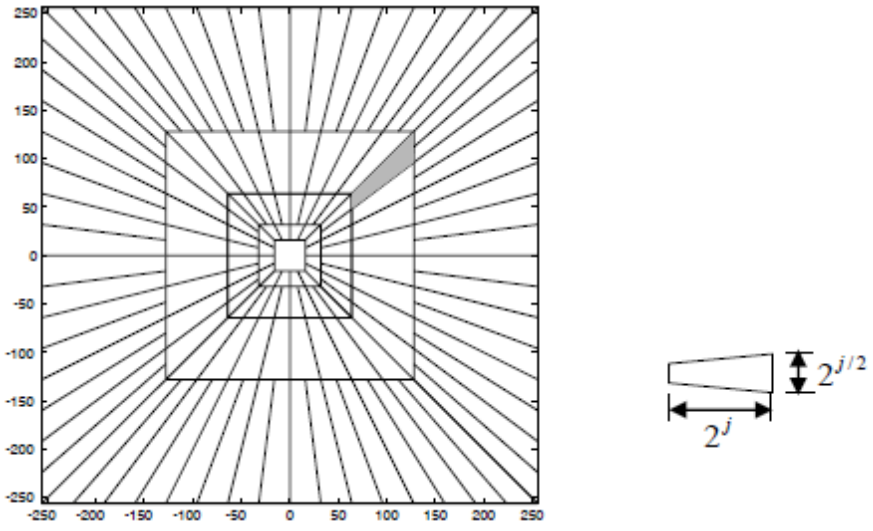

(a) (b)

Figure 2.5: (a) Frequency tiling of whole image by curvelet transform in discrete domain (b) Support of a curvelet at scale *j* in frequency domain showing its length and width.

Discrete curvelet transform of a two dimensional image $f[m,n]$ $(0 \leq m \leq M-1, 0 \leq n \leq N-1)$ at a given scale, orientation, and position is given by

$$c^D(j,l,k) := \sum_{\substack{0 \leq m < M, \\ 0 \leq n < N}} f[m,n]\overline{\varphi^D_{j,l,k}[m,n]}$$

where $c^D(j,l,k)$ is the curvelet coefficient at scale j, orientation l, and position $k[k_1,k_2]$. In the above equation $\varphi^D_{j,l,k}[m,n]$ is the digital curvelet waveform. In the frequency domain the mother curvelet is represented as a product of two windows, radial and angular windows as given by,

$$\widetilde{U_{j,l}}(\omega) := \widetilde{W_j}(\omega)V_j(\omega)$$

In the above equation $V_j\ (\omega)$ is a smooth, real valued, and non negative angular window obeying the admissibility conditions and $\widetilde{W_j}(\omega)$ is the cartesian equivalent of radial window, supported on concentric squares and is given by

$$\widetilde{W_j}(\omega) = \sqrt{\phi_{j+1}^2(\omega) - \phi_j^2(\omega)}\ , j \geq 0$$

where ϕ is defined as the product of low pass one dimensional windows given by

$$\phi_j(\omega_1, \omega_2) = \phi\left(2^{-j}\,\omega_1\right)\phi(2^{-j}\,\omega_2)$$

Function ϕ is equal to 1 in [-1/2,1/2] and vanishes outside [-2,2].Using the window $\widetilde{W_j}(\omega)$ we can separate the scales of the frequency plane. The angular localization is obtained using $V_j(\omega)$. The product of $V_j(\omega)$ and $\widetilde{W_j}(\omega)$ isolates the frequencies near the wedge $2^j \leq \omega_1 \leq 2^{j+1}$, $-2^{-j/2} \leq \omega_2 \leq 2^{j/2}$ [13]. In the frequency domainIn curvelet coefficient can be obtained as [20]

$$Curvelet\ Coefficient = IFFT[\ FFT(Curvelet)\ x\ FFT(Image)]$$

where IFFT is the inverse fast Fourier transform and FFT is the fast Fourier transform. The digital curvelet waveform in frequency domain is obtained by the product of two windows, called radial window and angular window. The support of the wedge like digital curvelet waveform is not rectangle and hence IFFT cannot be applied to the product to find the curvelet coefficient. A wrapping technique has been developed by Cand`es et al. [13] to solve this problem. The idea behind the wrapping technique is to select a parallelogram that can support the wedge shaped digital curvelet waveform and

wrap the parallelogram around the origin to obtain a rectangular support to apply IFFT. The wrapping technique is explained in Fig. 2.7.

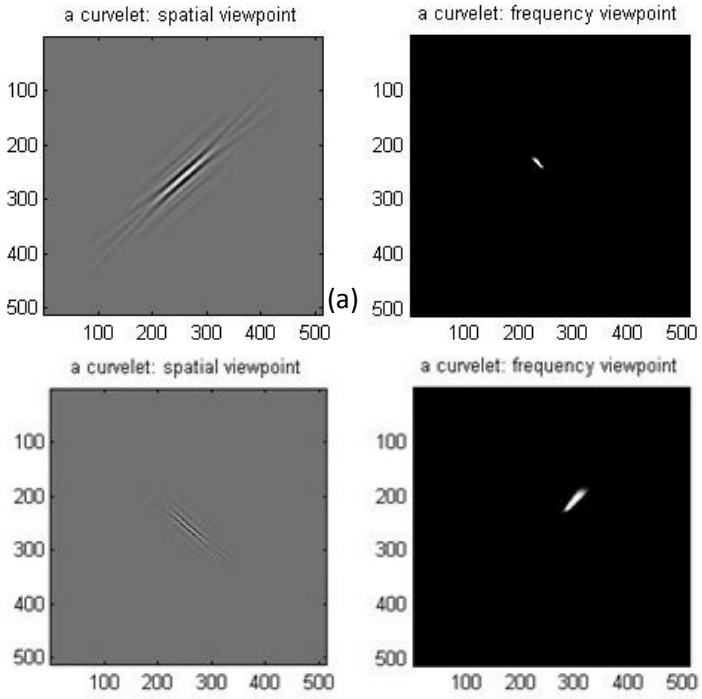

Figure 2.6: (a) Curvelet at scale 3 and orientation 1. (b) Curvelet at scale 4 and orientation 8. Left images are in spatial view and right side images are in frequency view.

The periodic tiling of the parallelogram results in a rectangular support at the center on which IFFT is obtained. The wrapping based curvelet transform is calculated as follows [13]:

a. Apply the 2D FFT and obtain Fourier samples $\hat{f}[m, n]$ of the image.

b. Find the product of Fourier domain digital curvelet waveform and the Fourier samples of the image.

c. Wrap the product around the origin to obtain rectangular support.

d. Apply the inverse 2D FFT on the wrapped product.

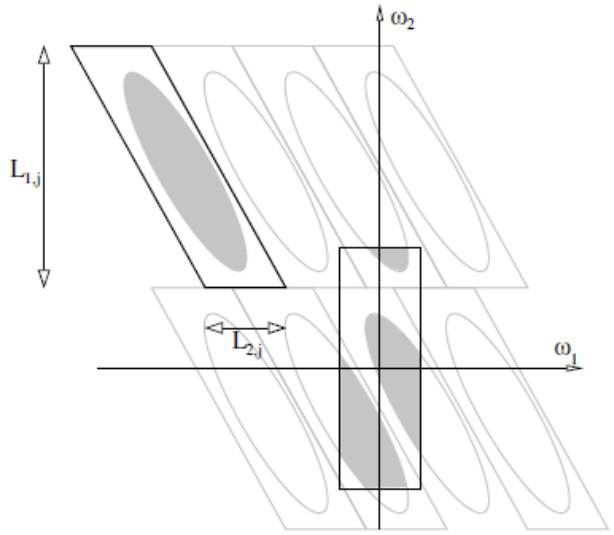

Figure 2.7: Wrapping method. The support in a parallelogram is finally into a rectangle (Reproduced from [13]).

This wrapping based curvelet transform is shown Fig.2.8.

To the best of author's knowledge, so far only one attempt [8] has been made to apply curvelet transform on palmprint. A modified first generation curvelet transform has been used to obtain the directional features. A two dimensional stationary discrete wavelet transform using discrete Mayer wavelet have been applied on the input palm image (of size 64 x 64) and four subbands were obtained. Ridgelet transform has been

applied on each subband to obtain curvelet coefficients. Finally hard thresholding has been applied on the curvelet coefficients.

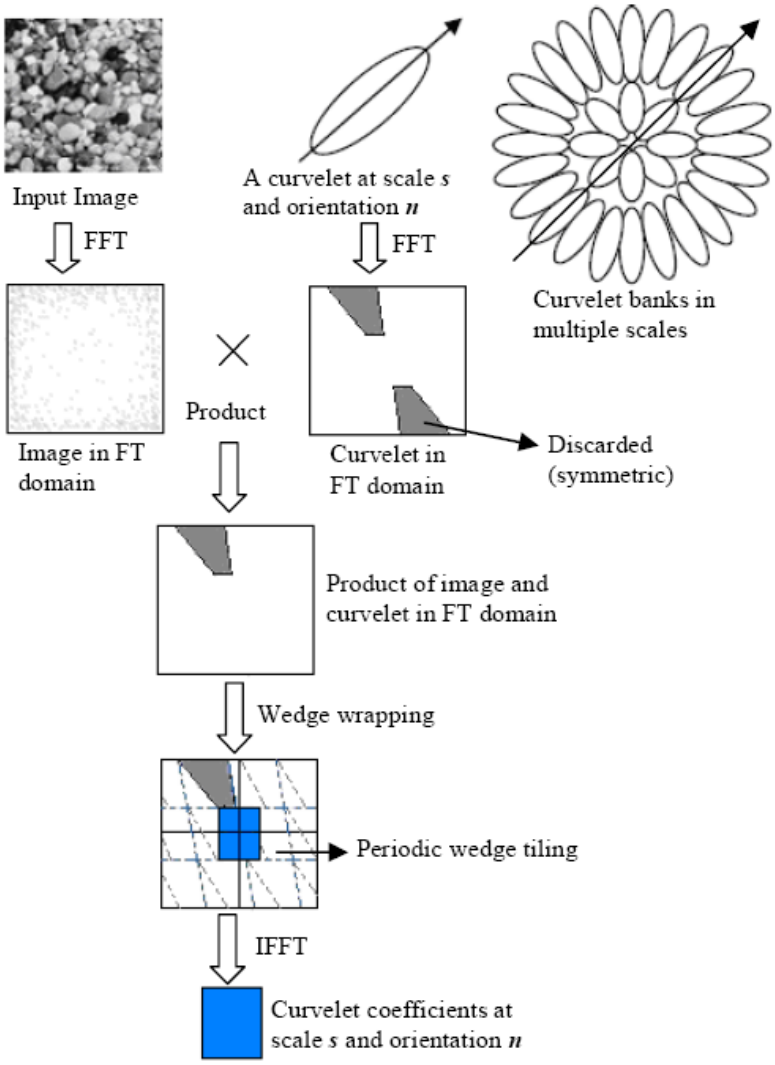

Figure 2.8: Curvelet transform using wrapping technique, reproduced from [21].

The magnitudes of the significant coefficients and their positions have been used as a feature vector. Euclidean distance was used as a classifier. The method has been tested

on a database of 600 samples and reports 95.5% recognition rate and high FAR and FRR values (6.25%). Moreover, the size of the curvelet coefficients is 65536 (4x128x128). After hard thresholding, even one percent of the coefficient and their positions form a high dimensional feature vector.

2.5 Details of Databases

In this section, the details of various databases used in this research are explained. Two types of biometric traits are used in this research, palm and face. Three publicly available palmprint databases and one face database are used for various experiments.

PolyU Palmprint Database [17]: PolyU palmprint database is a large publicly available database collected at Hongkong Polytechnic University. There are 7752 images collected 386 different palms. On average 20 images are collected from each palm. The 20 images are collected in two different sessions. In each session ten images are collected. The average time interval between two sessions is 69 days. Maximum time difference is 162 days and the minimum time difference is 4 days [5]. The light source and camera focus are changed for the second session images. The resolution of the images is 384 x 284 at 75 dpi. A fixed pegs structure has been used to collect the images. Some examples of the PolyU palm images are given in Fig. 2.9 and Fig. 2.10. In Fig. 2.9 different samples from different palm images are shown. It can be observed that both left and right hand palm images are available. Fig. 2.10 shows the two different samples of a palm collected in two different sessions. The variations in illumination can be observed from these images.

IIT Delhi Touchless Palmprint Database [15], [16]: IIT Delhi database contains hand images collected from touchless imaging setup. There are samples from 235 persons, each one providing 5 samples on average. All the images are bit map images of resolution 800x600 pixels. There are scale and rotation variations because of touch less imaging setup. Some sample images are shown in Fig. 2.11. Variations in scale, orientation and illumination can be observed in these images. The scale and rotation changes are high compared to the PolyU database.

GPDS Hand Database [18]: GPDS hand database contains 1440 images collected form 144 persons. Ten samples are collected from each person. Images have been collected using a desktop scanner at a resolution of 120 dpi. No pegs or templates have been used in imaging. Fig. 2.12 shows some sample images from GPDS database. There are some rotations in the images, but no scale changes because of a scanning surface.

AT & T Face Database (formerly the ORL database of faces) [19]: AT & T face database contains frontal face images of 40 different persons collected at the AT & T laboratories of Cambridge University. Each person provided 10 sample images, taken at different times, different lighting conditions, different expressions and different facial details [19]. Fig. 2.13 shows the sample images from the AT & T database. Variations in pose and expressions can be observed in this figure.

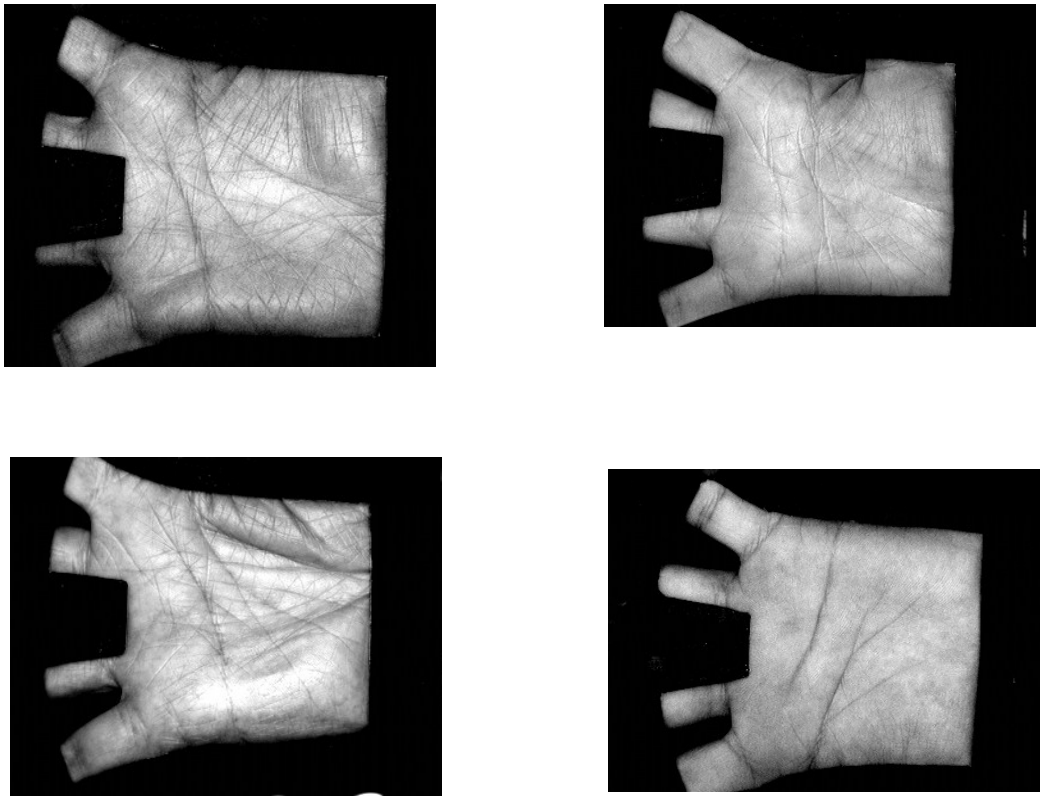

Figure 2.9: Sample images from the PolyU palmprint database.

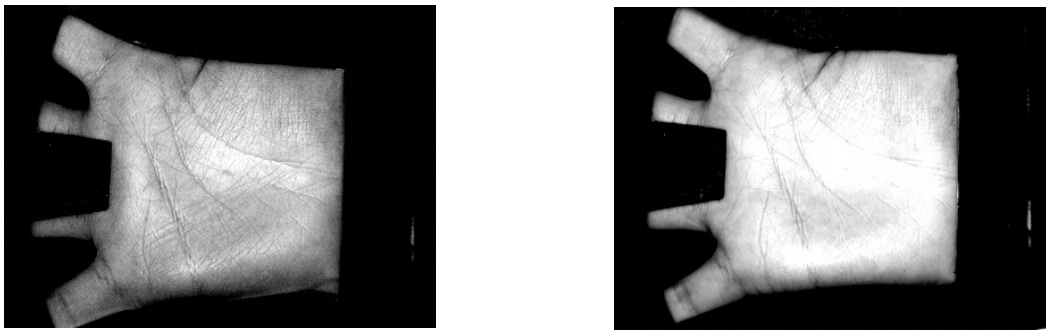

Figure 2.10: Two different samples of same person in two session of the PolyU palmprint database.

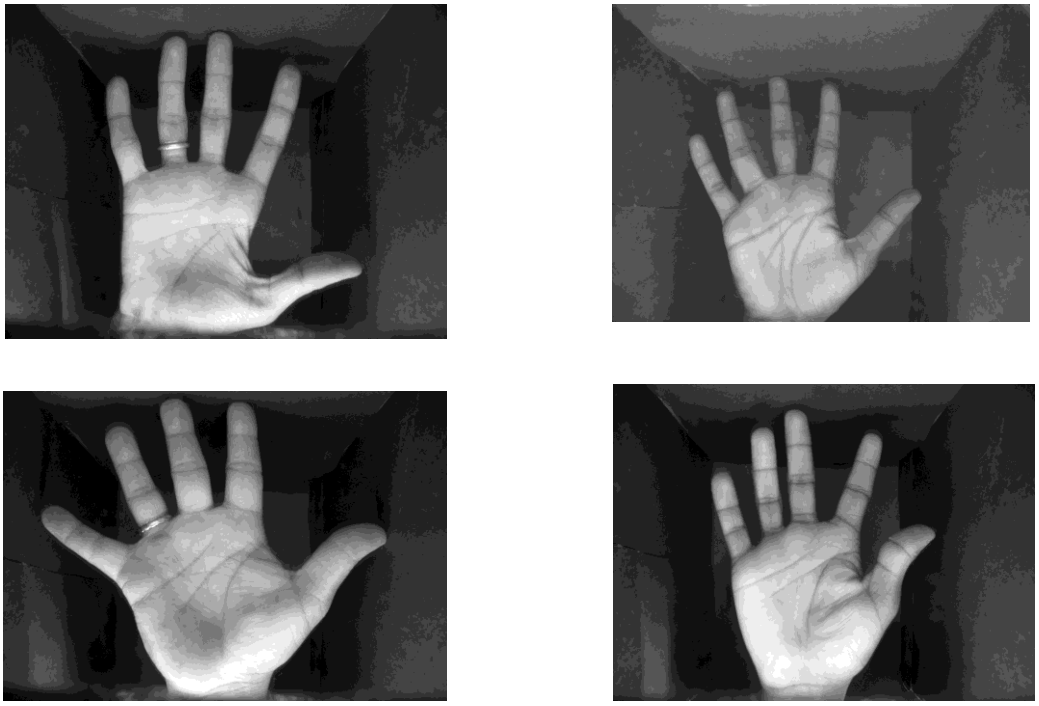

Figure 2.11: Sample images from the IIT Delhi palmprint database.

Figure 2.12: Sample images from the GPDS hand database.

Figure 2.13: Sample images from the AT & T face database.

Chapter 3

Curvelet Transform Techniques for Uni-modal and Bi-modal Biometric Systems

Two curvelet transform-based methods for biometric person identification are proposed in this chapter. The first method is for a palmprint-based uni-modal biometric system and the second method is for a bi-modal biometric system using face and palm. In uni-modal system, a binary code using curvelet directional subband images of a palm is obtained to represent the structure of the palm lines. A pixel-level fusion scheme using face and palm is proposed for a bi-modal system to improve the performance of eigenfaces [29] and eigenpalms.

3.1 Feature Extraction Technique for Palmprint Based Uni-modal Biometric System

Important palm lines in low resolution images and their structural details are discussed in Section 1.1 and it was discussed that a multi-scale and multi-directional representation is desirable in feature extraction. It was argued that the use of curvelet transform is worth investigating in extracting palm line features. In this section, a curvelet transform-based technique to extract palm line features is proposed.

Fig. 3.1 shows a cropped palmprint image and its curvelet transform. This transformed image is obtained by decomposing the image into 3 scales, decomposing scale 2 into 16

directions and scale 3 into 32 directions. The low pass image and directional bandpass images are arranged in a nice format for the display. The curvelet tool box [28] is used to calculate and display the curvelet transformed image. Because of the symmetry of the directional bandpass images, at each scale only one half of the directional bandpass images are sufficient for feature extraction. Fig. 3.2 shows how the directional bandpass images are directly related to the curve and line features of the input palm image. From this figure, it can be seen that one of the principal lines is related to the large magnitude curvelet coefficients at 3^{rd} scale and 3^{rd} orientation. The arrows in this figure connect the corresponding lines and the curvelet coefficients. Fig. 3.3 shows the optimal sparse representation of the curvelet transform. The image in Fig. 3.3a is the original preprocessed palm image. The curvelet transform of the original image is computed and a threshold is used to keep only 10% of the total coefficients. Inverse curvelet transform of these thresholded coefficients is obtained and shown in Fig. 3.3b. Since only 10% coefficients are used and the strong lines of the input image are recovered in Fig. 3.3b, it is clear that curve singularities are represented by a very small percentage of the curvelet coefficients. These features of curvelet transform clearly indicate that curvelet transform is a good choice for the palmprint representation.

3.1.1 Feature Extraction

If a given palm image of size 128 × 128 is decomposed into 5 scales, 8 directions at scale 2, 16 directions at scale 3, and 16 directions at scale 4, then, after excluding redundant

directional bandpass images, there are 20 directional bandpass images for feature extraction.

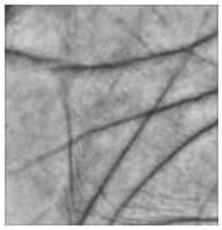

(a)

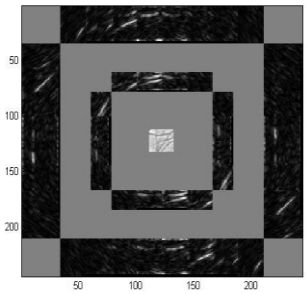

(b)

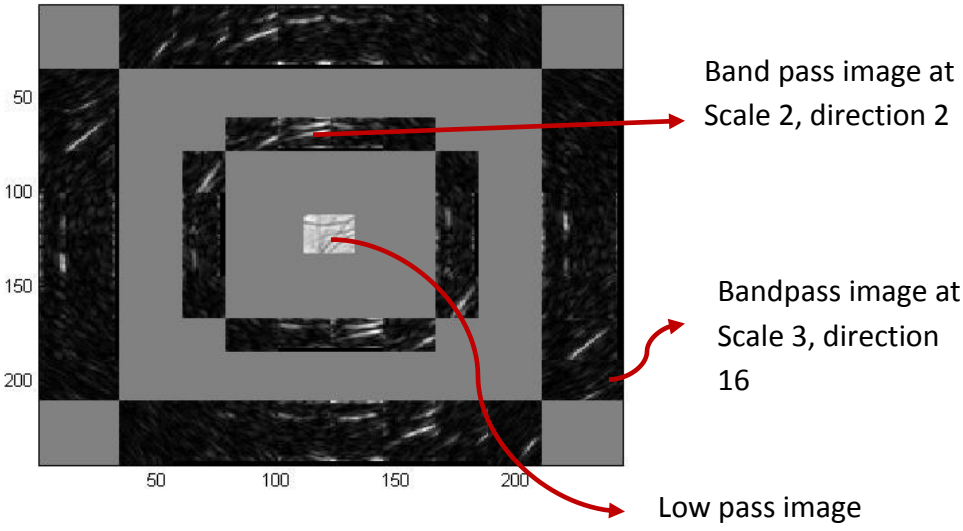

(c)

Figure 3.1: (a) A preprocessed palm image. (b) The curvelet transform of the palm image (c) Showing lowpass and directional bandpass images in the curvelet transform.

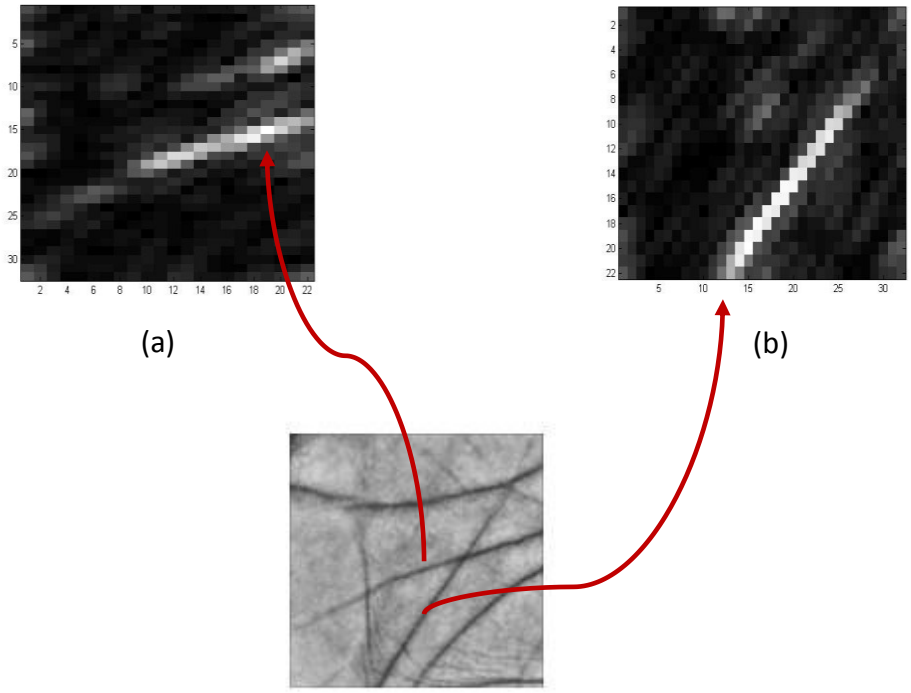

Figure 3.2: (a) A directional subband at scale 3 and direction 3, (b) A directional subband at scale 3 and direction 15 and (c) Corresponding palm image. Arrows show the corresponding directional features of the input palm image.

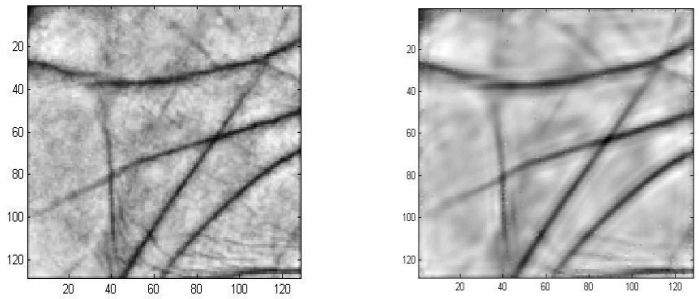

Figure 3.3: (a) Original palm image (b) Palm image reconstructed with 10 % of the curvelet coefficients.

The size of the directional bandpass image varies from scale to scale, for example, at scale 2 there are 4 bandpass images with size 10 × 21 and 4 with size 21 × 10. Similarly at scale 4, four bandpass images of size 35 × 44, 4 images of size 32 × 42, 4 of size 42 × 32 and 4 of size 44 × 35. Extracting the directional line features from these bandpass images and representing in a compact form is a major problem. Here a simple and very effective binary coding scheme is presented to represent the information in directional bandpass images. The method consists of the following steps.

Algorithm 1: Generation of Palm Curvelet Code (PCC)

Step 1 Decompose the preprocessed palm image into a fixed number of scales and directions.

Step 2 Downsample each directional bandpass image by a factor δ. This downsampling reduces the size of the feature vector. The range of δ depends on the size of the directional bandpass image.

Step 3 Keep only pre-specified percentage, say κ%, of the coefficients in each directional bandpass image, since the lines and curves are represented by a small number of the curvelet coefficients.

Step 4 Divide each row of the downsampled significant coefficient matrix into preset number of blocks β.

Step 5 Each block in a row is coded into a zero or a one. Each block is encoded to zero if all the coefficients in that block are zero. Block is encoded to one if

there is at least one non-zero coefficient. If the downsampled matrix is of size M × N, then the length of the code is Mβ bits.

Step 6 Repeat the steps 3 to 5 column wise, i.e., divide each column of the matrix into k blocks and encode each block. If the downsampled matrix is of size M × N, then the length of the code is βN bits.

Both the row and column codes can represent the structure of the directional bandpass image in a compact form. A directional bandpass image of size M × N is represented by B bytes where B is (Mβ +βN)/8. The value of β can be between 2 to 5 depending on the size of the matrix and is fixed for each scale. The significant coefficient percentage κ is between 5%-20%. All the directional bandpass images need not be downsampled, only those at higher scales can be downsampled to reduce the size of the code and δ can be in the range 0.6-1.

A PCC is obtained by concatenating row and column codes of the entire directional bandpass images. Length of PCC is in hundreds of bytes. Fig. 3.4(a) shows a downsampled significant coefficients directional bandpass image. This image is obtained by keeping only 15% of the coefficients and downsampling by 0.6. Fig. 3.4(b) is the row code obtained by dividing each row into 5 blocks and Fig. 3.4 (c) is the column code obtained by dividing each column into 5 blocks. By changing the number of scales of decomposition, number of directions at each scale, and downsample ratio different lengths of the feature vector can be obtained. For example, a 344 bytes PCC can be obtained for a 128 × 128 size palm image (by selecting number of scales = 5, number of

directions = [1,8,16,16,1], β = [1,2,2,5,1], and δ = [1,1,1,0.6,1]). If the number of directions at each scale is increased, then the palm lines are observed with high angular resolution. This may result in increase of intra class variations. Therefore the number of decomposition scales and directions are empirically selected based on the resolution of the input palm image.

3.1.2 Matching

The PCC is a binary code and hence a binary distance metric is used to find the distance between the two codes. There are many binary distance metrics in the literature [30]. Most of these metrics, such as Hamming distance and Jaccard dissimilarity are based on the total number of mismatches. Experiments have been conducted on palm databases to evaluate the performance of Jaccard and Hamming distance metrics. A significant improvement in verification rates has been observed with Jaccard distance metric, and hence Jaccard dissimilarity has been selected as a distance metric to match palmprints.

If *X* and Y are two binary vectors and S_{10}, S_{01}, and S_{11} are the mismatch and matching counts defined as follows,

$$S_{10} = No.of\ times\ (X = 1\ and\ Y = 0)$$

$$S_{01} = No.of\ times\ (X = 0\ and\ Y = 1)$$

$$S_{11} = No.of\ times\ (X = 1\ and\ Y = 1)$$

then, the Jaccard dissimilarity or distance between the two binary vectors can be defined as

$$JD(X,Y) = \frac{S_{10} + S_{01}}{S_{10} + S_{01} + S_{11}}$$

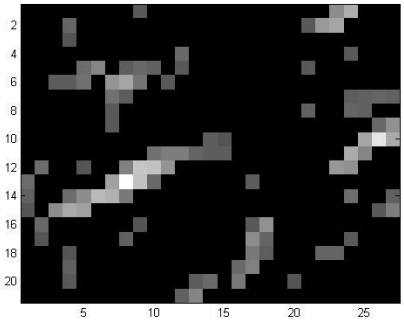

(a)

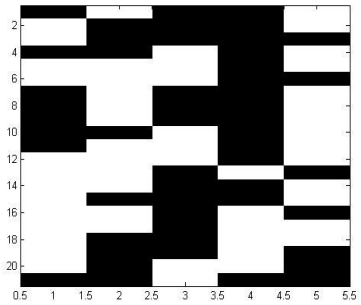

(b)

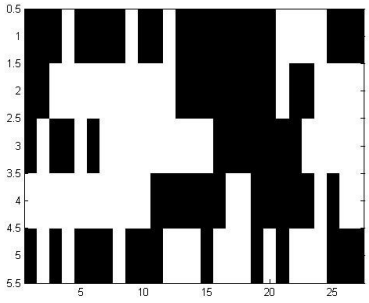

(c)

Figure 3.4: (a) A downsampled, significant coefficient directional subband, (b) its row code, and (c) its column code.

The Jaccard distance is calculated for the given two PCCs. The score should be zero if both the palm images are from the same class. But practically zero score is not possible because of the intra class variations.

3.1.3 Hierarchical Identification using PCC

Palmprint identification in large size databases is a time consuming process; hence a guided search with multiple features will be appropriate for improving the speed of the identification process. The proposed PCC can be used in a guided search. The proposed code is calculated for different scales and different directions. The code at each scale can be used to eliminate some percentage of samples of the large database. Since the PCC is obtained using scale 2 to scale 4 CDSCs, there can be two levels in a guided search. The hierarchical identification using PCC is described in the following steps.

Algorithm 2: Guided Search using PCC

Step 1 Search the registration database with the scale 2 feature vector. Obtain subset 1, that contains the feature vectors from the registration database with a matching score less than or equal to a preset threshold T_1.

Step 2 Search the subset 1 using scale 3 feature vector and a preset threshold T_2, to obtain subset 2.

Step 3 Finally, use the scale 4 feature vector and a threshold T_3 to select a sample from the subset 2.

The number of directions at scale 2 is one half of those at scale 3 and the size of the directional bandpass images is also small at scale 2 and hence only a small percentage of bytes of the PCC are used in the first level identification. This process saves the identification time.

If τ_1 is the time required for a matching by the scale 2 feature vector, τ_2 and τ_3 are the times required for a matching by those feature vectors at scale 3 and scale 4 and D is the size of the registration database, then, hierarchical identification takes a time I_T given as follows

$$I_T = D \times \tau_1 + (D-E_1) \times \tau_2 + (D-E_1-E_2) \times \tau_3$$

where E_1 is the number of the samples eliminated by scale 2 feature vector and E_2 is the number of samples eliminated by the scale 3 feature vector.

3.2 A Bi-modal Biometric System using Pixel-level Fusion of Face and Palm

Multimodal biometric systems have gained much concentration over the past few years. In multimodal biometric systems different biometric traits are fused to improve the performance of the system. Fusion is carried at different levels of an identification system. In [24], information fusion in biometrics is broadly classified into two categories, pre-classification fusion and post-classification fusion.

In Pre-classification fusion, the information is fused before applying a classifier. This fusion can be at sensor level or at feature level. In sensor level fusion, different sensor outputs are combined. This sensor level fusion may not be feasible for all the cases. The output data of the sensors must be compatible. In feature level fusion, the information is fused after the feature extraction. This can be simple feature concatenation or weighted summation [25]. In the post-classification fusion, the decision information

from different classifiers is combined to improve the system performance. In this section the author concentrates on pre-classification fusion.

In this section a pixel-level fusion scheme for face and palmprint using curvelet transform is proposed. The method is given as follows:

Algorithm 3: Pixel- level Fusion of Face and Palm

Step 1 Enhance the cropped palm image to elevate the palm lines and to reduce the effect of back ground illumination.

Step 2 Apply a Gaussian smoothing filter and enhance the palm image using adaptive histogram equalization.

Step 3 Resize the palm image to match with the face image size using bicubic interpolation [39].

Step 4 Obtain the curvelet transform of the face and the processed palmprint images for a fixed number of scales and directions.

Step 5 Apply the fusion rule for the lowpass image and each directional bandpass image of face and palm.

Step 6 Find the inverse curvelet transform and obtain the fused face and palmprint image.

Step 7 Take the absolute values of the resultant image and normalize the image. If I is the image obtained by the inverse curvelet transform then normalized image can be obtained as

$$I(m,n) = \frac{I(m,n) - I_{min}}{I_{max} - I_{min}} \text{ x } L$$

In the above equation, I_{min} is the minimum value of the image I, I_{max} is the maximum value of I, L is the maximum value of the gray scale range (255) and m, n are the coordinates of the pixel.

Step 8 Downsample the fused images to 30 × 30 to reduce computational cost in feature extraction.

The fusion process is shown in Fig. 3.5. Fusion rule is a function that takes two curvelet coefficients of the face and the palm and produces a resultant curvelet coefficient. If the function calculates the mean of the two coefficients, then it is called *mean fusion rule*; if the function results in the maximum of the two coefficients, then the rule is *max fusion rule*, similarly *min fusion rule* results in the minimum of the two coefficients. Curvelet transform produces lowpass image and directional bandpass images, two different fusion rules can be selected for lowpass images and bandpass images and hence different fusion rules can be formulated. In *mean-mean fusion rule, mean fusion rule* is applied for both lowpass and directional bandpass images, similarly in *max-mean fusion rule, max fusion rule* is applied on lowpass image and *mean fusion rule* is applied on directional bandpass images. Some other possibilities are *max-max*, *mean-max* and min-*min fusion rule*. Fig. 3.6 shows the mean fusion rule for lowpass images and Fig. 3.7 shows the same fusion rule for directional bandpass images. Finally inverse curvelet transform results in a fused face and palm image and the resultant image is normalized to the gray scale range. Some sample fused images using *mean-mean fusion rule* are

shown Fig. 3.8. From these images it can be seen that both face and palm features are available in the fused image.

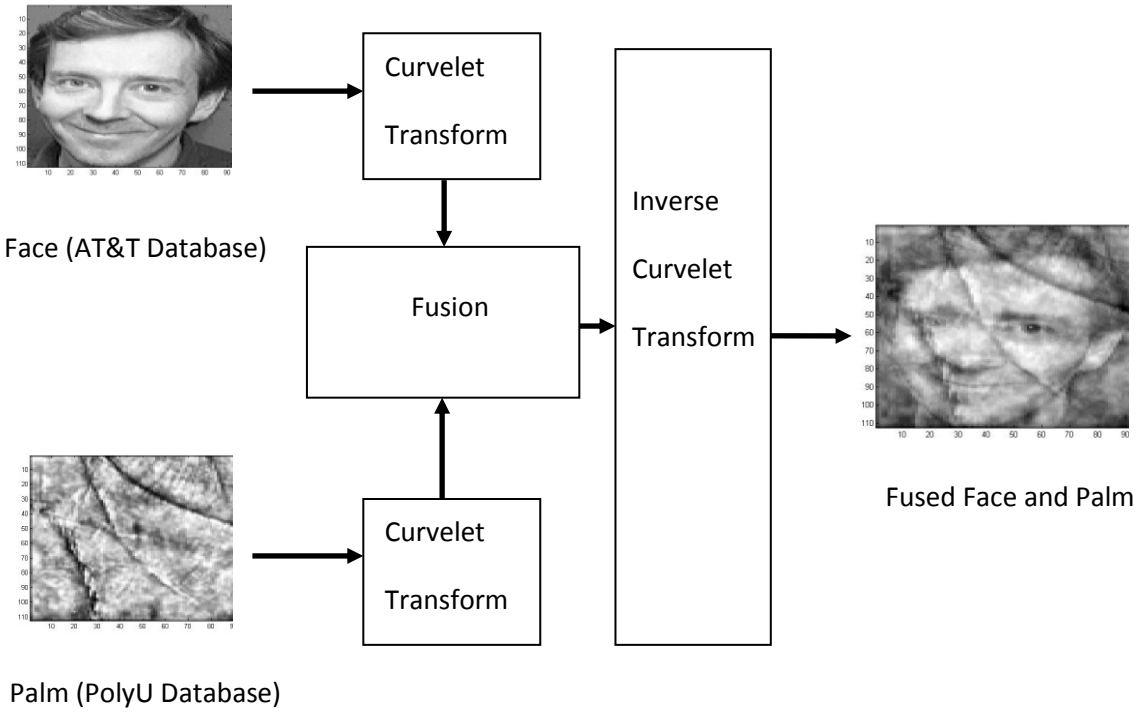

Figure 3.5: Fusion in curvelet transform domain.

3.2.1 Feature Extraction and Matching

Subspace methods, such as principal component analysis (PCA) and independent component analysis (ICA) have been already proven to be successful in face recognition [29], [32]. In this thesis, PCA method is used to classify the fused face and palmprint images. PCA is a dimensionality reduction technique that transforms the large number of correlated variables into a small set of uncorrelated variables. These uncorrelated variables are called principal components [31]. These principal components are the

eigen vectors of the covariance matrix. Eigen vectors with non-zero eigen values produce orthonormal basis for the given feature space.

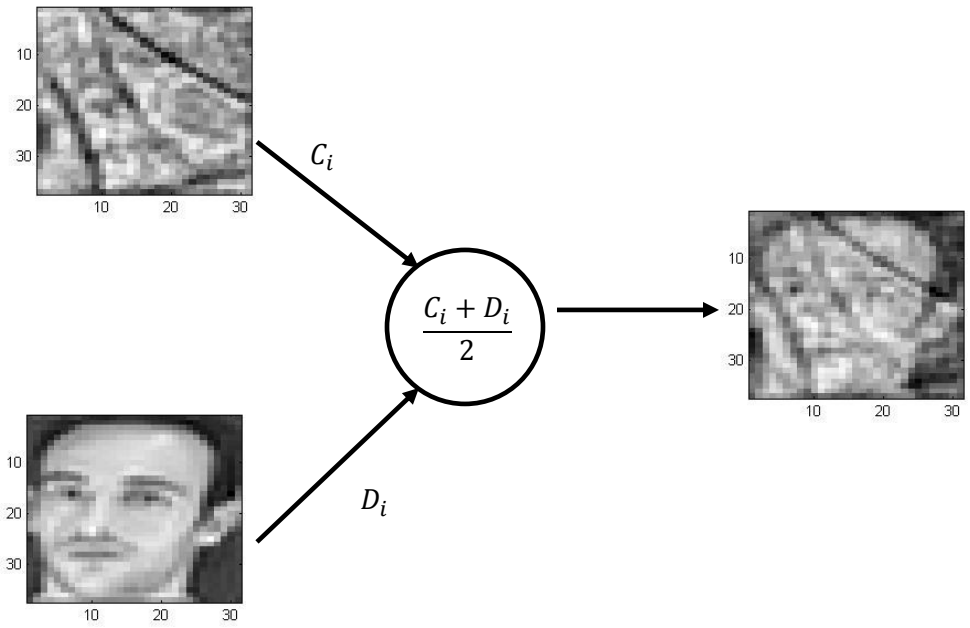

Figure 3.6: Mean fusion of lowpass face and palm images.

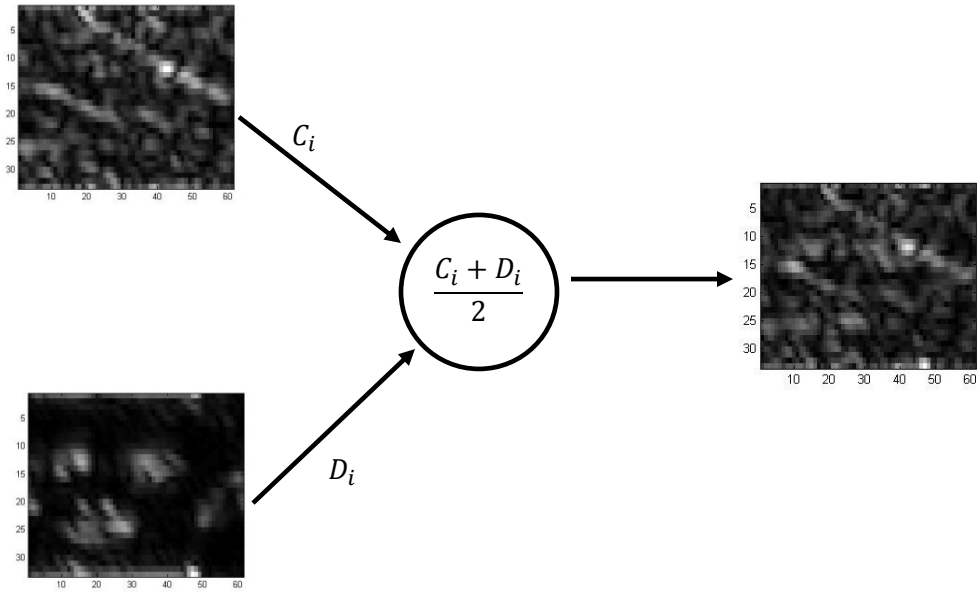

Figure 3.7: Mean fusion of directional bandpass face and palm images.

Figure 3.8: Samples of some fused images.

The dimensionality reduction can be achieved by selecting a subset of eigen vectors that correspond to the largest eigen values. The PCA algorithm can be summarized as below:

a. Convert all the training images into column vectors. Let the training set of fused images be $I_1, I_2, I_3, \ldots, I_M$ where M is the number of training samples. Then the size of each column vector I_x is $N^2 \times 1$.

b. Calculate the average of the training set denoted by, ψ, as given below:

$$\psi = (\frac{1}{M}) \sum_{n=1}^{M} I_n$$

c. Calculate χ_i for each image I_i, where χ_i is the difference between image I_i and the average image ψ.

$$\chi_i = I_i - \psi$$

d. Obtain the covariance matrix of χ

$$C = \left(\frac{1}{M}\right) \sum_{n=1}^{M} \chi_n \chi_n^T = AA^T$$

where $A = [\chi_1, \chi_2, \ldots, \chi_M]$.

e. Calculate the eigen vectors of C. The size of the matrix C is $N^2 \times N^2$. Since N^2 is the size of the image, it is very complicated and time consuming to calculate the eigen vectors of such a large matrix. Therefore the eigen vectors ϑ, of the matrix $A^T A$ with size M x M are calculated [29].

f. Calculate the M eigen vectors of AA^T as given below:

$$U_l = \sum_{k=1}^{M} \vartheta_{lk} \chi_k \qquad l = 1,2,3 \ldots M$$

g. Normalize the eigen vectors to improve the classification accuracy [37]. Choose M' eigen vectors associated with M' largest eigen values to define the feature space [29].

h. Project the training samples on to this space and calculate the weight vectors. These weight vectors along with M' eigen vectors form the feature space. The weight vector of a training image I_i is calculated as follows

$$\Omega^T = [\omega_1, \omega_2, \ldots, \omega_{M'}]$$

where $\omega_k = U_k^T \chi_i$ for k = 1,2,...,M'.

3.2.2 Recognition

When a new query test sample is given, its difference from average space is calculated and its weight vector is calculated by projection. This weight vector is compared with the weight vectors of the training samples by calculating the Euclidian distance to

identify the test sample. If X and Y are the two weight vectors of the test and training samples, then the Euclidean distance S is calculated as follows

$$S = \sqrt{\sum_{i=1}^{M'} (X_i - Y_i)^2}$$

where M' is the length of the feature vector. The training class, that results in a minimum Euclidean distance is assigned to the test sample.

3.3 Summary

In this chapter advantages of curvelet transform and its ability to represent curve features are explained with examples. The problem of feature extraction using the directional bandpass images has been discussed. A simple binary coding technique has been proposed to generate PCC and the use of PCC in hierarchical identification has also been discussed. A second method in curvelet transform domain for a bi-modal biometric system using pixel-level fusion of face and palm has been proposed.

Chapter 4

Experiments and Analysis

Two techniques in curvelet transform domain for biometric person identification have been proposed in Chapter 3. In this chapter, comprehensive set of experiments are conducted to evaluate the performance of the proposed methods and the details of the experiments, results and analysis of the two proposed methods are presented.

4.1 Experiments on Palmprint Based Uni-modal System

The performance of the proposed method for palmprint based uni-modal biometric system is tested on three different palmprint databases. The details of the three palmprint databases and the methods of preprocessing have been explained in Chapter 2. Performance is tested for the two modes of the biometric system, namely, identification and verification. Identification and verification experiments are conducted on all the three databases. Since the resolution and method of image acquisition of the three palm databases are different, various experiments are conducted by changing the parameters of the curvelet transform and the coding scheme. The parameter set that gives the best performance is selected for each database. Two sets of parameters are selected for the three databases. Two feature vectors of lengths 344 bytes and 380 bytes are generated using these parameter sets. The parameters used in the extraction of the feature vectors and the lengths of the resulting feature vectors are given in Table

4.1. It can be observed from this table that the two feature vectors differ in angular resolution, downsample ratio, and the number of coding blocks. The angular resolution for 380-byte PCC is twice that of 344-byte PCC. Experimental results on PCCs of lengths 398.5, 366, 381.5, and 342.5 are also presented to study the effects of the variations in the lengths of the feature vectors on the performance. The experiments are divided into three parts. In part 1, experiments are conducted to evaluate the performance of the proposed method on person identification without hierarchy, whereas part 2 experiments are on the person identification with hierarchy. In part 3, experiments are conducted to evaluate the performance of the proposed method on the palmprint verification.

Table 4.1: Two parameter sets to generate 344 and 380-byte PCC.

Parameters	Values	
	380-byte PCC	344-byte PCC
Number of scales	5	5
Number of directions	[1,16,32,32,1]	[1,8,16,16,1]
Downsample ratio (δ) at each scale	[1,1,0.7,0.5,1]	[1,1,1,0.6,1]
Percentage of significant coefficients (κ) to keep at each scale	[100,15,10,8,100]	[100,15,20,18,100]
Number of blocks (β)	[-,2,3,4,-]*	[-,2,2,5,-]*

*Hyphen (-) indicates that the scales are not used in the coding scheme.

4.1.1 Experiments on Identification without Hierarchy

In these experiments, the databases are divided into training and test databases. Three tests are performed by changing the number of training samples from 1 to 3. Results are obtained for all the possible training sets and the average values of the identification results along with their standard deviations are presented. If the total number of samples in each class is N_{SC} and the number of training samples is N_{TS} then there are N_{TE} ways to select these N_{TS} samples as given by

$$N_{TE} = \binom{N_{SC}}{N_{TS}} = \frac{N_{SC}!}{(N_{SC}-N_{TS})! \times (N_{TS})!}$$

As discussed in Chapter 2, the images in the PolyU database have been collected in 2 sessions, and hence, the training samples are taken from only session 1 for a thorough testing. Two different test sets are formed for the PolyU palm database. Test set 1 contains all the images except for the training samples. Test set 2 contains only the images collected in session 2. For example, there are 362 classes of different palms with 20 samples for each palm. If the number of training samples (N_{TS}) is 3, then, Test set 1 contains 17 x 362 images whereas Test set 2 contains 10 x 362 images of each class. There are no exact details of the time delays among the samples for GPDS and IIT Delhi databases; hence, there are no special test cases for these two databases.

Table 4.2 gives the average identification results using Test set 1 of the PolyU database for different numbers of training samples. CIR, FIR and FRR are calculated as given in Section 2.3. It can be seen from this table that very high identification rates even with

small training sample size are possible with the proposed method. It should be noted that these results are not the best-case results. They are the average of the all possible sample sets collected from only session 1. For example, when the number of training samples is set to 2, two samples are selected from session 1 which can be done in 45 ways (selecting 10 out of 2). The average of all the 45 test cases is calculated. In the case of a single training sample set, the samples are collected from both the sessions, and hence, there are 20 possible training sets. It can also be observed from Table 4.2 that the deviation from the average rate is also very small indicating a constant performance for all possible sample sets. Table 4.3 gives the identification results using Test set 2, where training samples are collected from session 1 and test samples are from session 2. This test is more appropriate to verify the performance on the PolyU database. In all these cases FRR is zero and low FIRs are obtained. Table 4.4 gives the best and the worst case CIRs of all the test cases for both the test sets.

Table 4.2: Identification results on the PolyU database with Test set 1 and 380-byte PCC.

Number of Training Samples	Average Rates and Standard Deviations			Threshold	Number of Experiments
	CIR	FIR	FRR		
1	98.06 ± 0.25	1.93 ±0.25	0	0.78	20
2	98.89 ± 0.17	1.10 ±0.17	0	0.78	45
3	99.17 ± 0.13	0.82 ± 0.13	0	0.78	120

Table 4.3: Identification results on the PolyU database with Test set 2 and 380-byte PCC.

Number of Training Samples	Average Rates and Standard Deviations			Threshold	Number of Experiments
	CIR	FIR	FRR		
1	96.51 ± 0.25	3.48 ±0.25	0	0.78	20
2	98.11 ± 0.27	1.88 ±0.27	0	0.78	45
3	98.63 ± 0.21	1.36 ± 0.21	0	0.78	120

Table 4.4: The best and the worst identification results on the PolyU database on Test set 1 and Test set -2 with 380 bytes PCC.

Number of Training Samples	The best and the worst CIR			
	Test set 1		Test set 2	
	The best CIR	The worst CIR	The best CIR	The worst CIR
1	98.73	97.74	96.85	96.07
2	99.26	98.40	98.67	97.37
3	99.52	98.68	99.19	97.97

Finally, the results comparing the proposed method with the other methods are presented in Table 4.5. Based on the training sets and number of experiments, it can be observed from this table that the proposed method gives the best identification results compared to other methods. The experiments are repeated on the GPDS and the IITD palm databases. Table 4.6 gives the average identification results and their standard deviations of the IITD database. The best and the worst CIRs of the IITD database are given in Table 4.7. The results on GPDS database are given in the tables 4.8 and 4.9. A consistent performance of the proposed PCC is observed form these tables. Experiments using different lengths of PCCs are also conducted on all the three databases and the results are given in Table 4.10. Parameter values used to generate these PCCs are given in table 4.11. The identification rates in the Table 4.10 are the average rates of all the possible training sets and the number of training samples is 3. It can be seen from this table that the changes in identification rates are very small for GPDS and IITD databases. The changes in the PolyU database are considerable for 344- byte PCC. The 344-byte PCC is obtained for an angular resolution of 8. It should be noted that the PolyU image resolution is 75 dpi. This shows that the selection of angular resolution depends on the

resolution of the input palm image. A low angular resolution for high resolution images and a high angular resolution for low resolution palm images is desirable.

Table 4.5: Identification results comparing the proposed method with the other methods on the PolyU database.

Method	Recognition Rate	Number of Training Samples	Number of Test Samples	Number of Classes /Number of Samples
[3]	99.50	800	200	200/5
[4]	98.00	50	150	50/4
[7]*	99.00	400	200	100/6
[6]*	97.00	400	200	100/6
[8]*	95.50	200	400	100/6
[33]	95.16	3860	3860	386/20
[33]	99.69	1544	2316	386/10 (images from session 2)
[34]	99.20	1800	1200	300/10
[5]	97.00	300	1700	100/20
Proposed method Test set 1	99.52 (99.17) †	1086	6154	362/20
Proposed method Test set 2	99.19 (98.63) †	1086	3620	362/20

*These methods used samples from both the sessions for training. †The rates are the average of the identification rates of 120 experiments.

Table 4.6: Identification results on the IITD database with 380-byte PCC.

Number of Training Samples	Average Rates and Standard Deviations			Threshold	Number of Experiments
	CIR	FIR	FRR		
1	89.53 ± 0.46	10.46 ± 0.46	0	0.78	5
2	95.51 ± 0.96	4.48 ± 0.96	0	0.78	10
3	97.42 ± 0.55	2.57 ± 0.55	0	0.78	10

Table 4.7: The best and the worst case identification results on the IITD database with 380-byte PCC.

Number of Training Samples	The best and the worst CIR	
	The best CIR	The worst CIR
1	90.29	89.19
2	96.92	93.85
3	98.30	96.35

Table 4.8: Identification results on the GPDS database with 344-byte PCC.

Number of Training Samples	Average Rates and Standard Deviations			Threshold	Number of Experiments
	CIR	FIR	FRR		
1	99.32 ± 0.32	0.67 ± 0.32	0	0.78	20
2	99.83 ± 0.11	0.16 ± 0.11	0	0.78	45
3	99.90 ± 0.08	0.10 ± 0.08	0	0.78	120

Table 4.9: The best and the worst case identification results on the GPDS database with 344-byte PCC.

Number of Training Samples	The best and the worst CIR	
	The best CIR	The worst CIR
1	99.76	98.84
2	100	99.56
3	100	99.70

In all these experiments, results are obtained using MATLAB code. To test the execution time of the proposed method, feature extraction and matching codes are written in C++ to test the identification results on the GPDS database. Intel OPENCV library [36] for image processing applications and curvelet tool box [28] are used for this test. For the same set of parameters, curvelet transform generates slightly different sizes of

bandpass images for MATLAB and C++ implementations, and hence, the PCCs slightly differ. For example, the parameter set that generates 344-byte PCC in MATLAB, gives a 353-byte PCC in C++, but there is very small deviation in the performance.

Table 4.10: Average recognition rates for all databases for different feature vectors. (Number of training samples is 3 for all these cases).

Database	PCC Length in Bytes (bits)	Average Rates		
		CIR	FIR	FRR
PolyU Test set 1	398.5 (3188)	98.92	1.07	0
PolyU Test set 2	398.5 (3188)	98.21	1.78	0
PolyU Test set 1	342.5 (2740)	99.01	0.98	0
PolyU Test set 2	342.5 (2740)	98.37	1.62	0
PolyU Test set 1	344 (2752)	98.14	1.85	0
PolyU Test set 2	344 (2752)	96.93	3.06	0
IITD	344 (2752)	97.01	2.98	0
IITD	398.5 (3188)	97.28	2.71	0
IITD	342.5 (2740)	97.13	2.86	0
GPDs	380 (3040)	99.80	0.19	0
GPDS	381.5 (3052)	99.92	0.07	0
GPDS	366 (2928)	99.88	0.11	0

Table 4.11: Parameter sets used to generate PCCs of different lengths.

Length of PCC	Number of Directions	β	δ	κ
398.5	[-,16,32,32,-]	[-,2,3,4,-]	[1,1,0.5,0.7,1]	[100,15,10,8,100]
342.5	[-,16,32,32,-]	[-,2,3,4,-]	[1,1,0.5,0.5,1]	[100,15,10,8,100]
381.5	[-,8,16,16,-]	[-,2,2,5,-]	[1,1,1,0.7,1]	[100,15,20,18,100]
366	[-,8,16,16,-]	[-,2,3,4,-]	[1,1,1,0.7,1]	[100,15,20,18,100]

Table 4.12 gives the details of the identification rates and the execution times for both the cases. All the experiments are conducted on windows machine with 1.86GHz processor speed and 1 GB RAM. MATLAB codes are tested in MATLAB R2007b.The execution time in C++ shows the feasibility of the PCC for real time applications. The execution time in C++ can be reduced further as the codes are not optimized.

Table 4.12: Results and execution times of the PCC on GPDS database with 3 training samples

Code	Average CIR	Best CIR	Feature Extraction Time	Feature Length
MATLAB	99.90	100	145 ms	344 bytes
C++	99.59	100	78 ms	353 bytes

4.1.2 Experiments on Identification with Hierarchy

In these experiments, hierarchical identification using the proposed method is tested. Three stage guided search scheme is selected using scale 2, scale 3 and scale 4 CDSCs. The threshold values are selected empirically and set to 0.65, 0.75 and 0.80 for scale 2, scale 3 and scale 4 CDSCs, respectively. Three experiments are conducted to test the performance of the guided search. In the first experiment the identification results for different number of training samples are obtained to compare the performance with and without hierarchical search. Table 4.13 gives the hierarchical identification results on the PolyU database with Test set 1 using 380-byte PCC. The recognition rates are the average values of all the possible test cases. Comparing Tables 4.2 and 4.13, it is clear

that identification rates of guided search are 0.97%, 1.45% and 2.91% less than those of without guided search for training samples 3, 2 and 1, respectively. In the second experiment, the percentage of eliminations by each stage are studied. For this purpose, the feature vector of every sample of the PolyU database is identified from the rest using guided search and the elimination percentage of each stage are noted. This process is repeated for all the samples of the PolyU database and the average of the eliminations is noted. Fig. 4.1.1 shows the bar plot of the elimination and candidate percentage at each level giving the best, average, and the worst elimination percentages. Scale 2 CDSCs can eliminate on average 80.6% of the registration samples and scale 3 CDSCs can eliminate 90.6% of the selected sample set by the scale 2 CDSCs. In this test each feature vector is compared with 7239 other feature vectors in a guided scheme. First stage eliminates approximately 6226 feature vectors leaving 1013 feature vectors for the second stage. In a 380-byte PCC, first stage requires only 39 bytes to eliminate 80% of the registration database. Second stage utilizes 123 bytes and the third stage utilizes remaining 218 bytes. This clearly indicates the effectiveness of the guided scheme with respect to the matching time. In third experiment, a large palm database is used to study the execution times of the identification methods, with and without hierarchy. A large palmprint database is not available, and hence, the three databases are combined to form a large database of size 9710 images. All the PolyU images are used as test samples. Each PolyU palm image is identified from other 9709 images using guided scheme. The time taken to identify all the PolyU images is calculated for both the identification methods, with and without hierarchy. The matching times in seconds are

given in Table 4.14. From this table it is clear that guided search saves 3 times of the time.

Table 4.13: Average identification rates of guided search on the PolyU database.

Number of Training Samples	CIR	FIR	FRR
1	95.20 ± 0.41	3.27 ± 0.29	1.71 ± 0.2
2	97.46 ± 0.25	1.76 ± 0.20	0.77 ± 0.1
3	98.22 ± 0.22	1.29 ± 0.16	0.48 ± 0.07

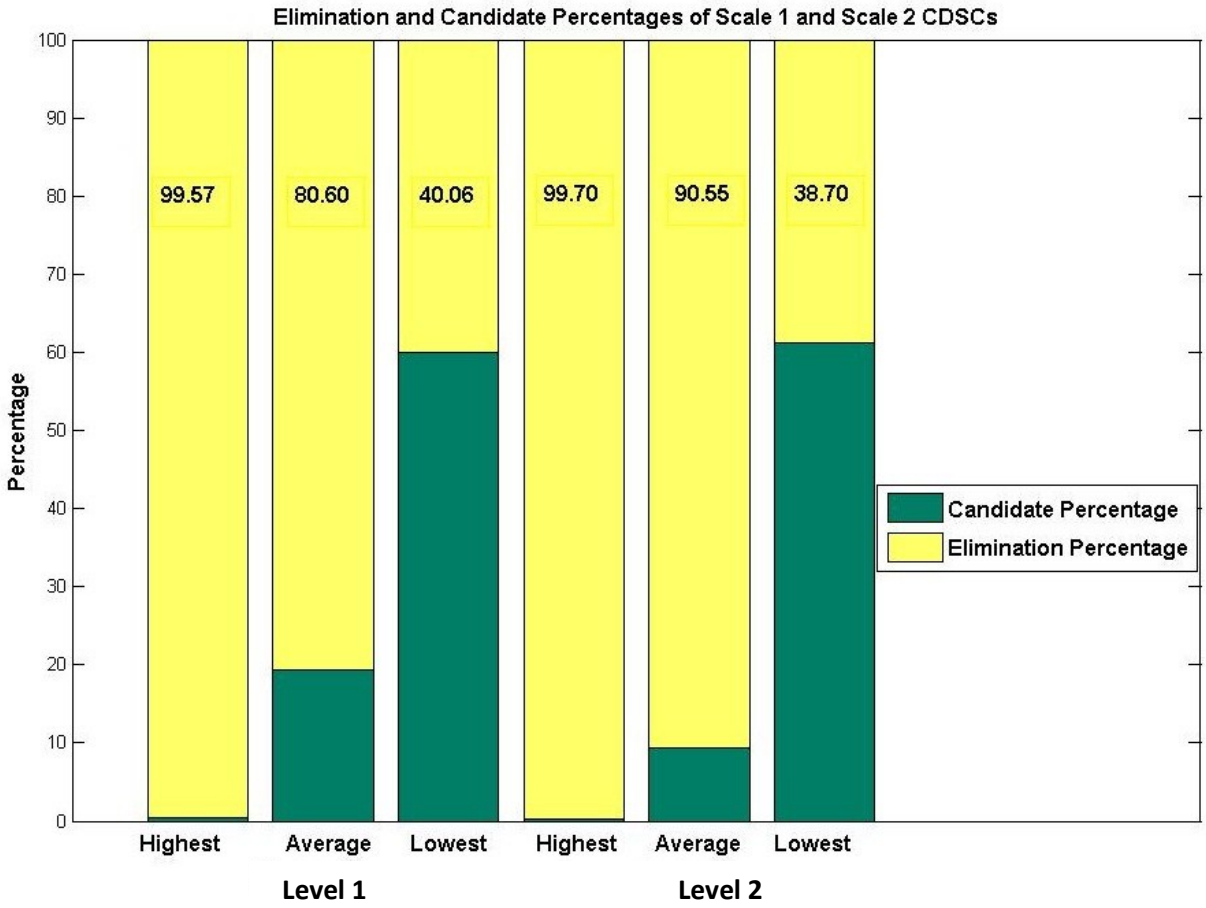

Figure 4.1: Elimination percentage and candidate percentage of the guided scheme at each level.

Table 4.14: Identification times with and without guided search for a large database.

Identification Method	Time in seconds	Remarks
Hierarchical	2047	Time is the total time taken to identify 7240 samples from a given registration database of size 9710. The method is tested in MATLAB R2007B, on a desktop with 1.86GHz speed and 1 GB RAM.
Without hierarchy	6395	

4.1.3 Experiments on Palm Verification

In these experiments, verification mode of the biometric system is tested using the proposed method. This test is conducted for all the three databases. Each image in the database is matched with every other image to calculate the genuine and imposter scores. If both the images are from the same class, the matching score is genuine otherwise the score is imposter. Since the preprocessing and ROI extraction is not perfect, there are some translational and rotational errors in the cropped images. These errors may increase the intra class variance and hence different ROIs of the same palm image are compared with each image in the database and the minimum of these scores is considered for the verification. In total, 9 ROIs are used in this process and are obtained by translating the center point of the first ROI into 8 directions by 5 pixels. All the genuine scores and imposter scores of a palm database are used for obtaining equal error rate (EER), receiver operating characteristics (ROC), and genuine acceptance rate (GAR). In the PolyU database there are 7240 images which accounts for 68780 genuine

scores and 26136400 imposter scores. In the GPDS database there are 1440 images that results in 6480 genuine scores and 1029600 imposter scores. Similarly there are 2060 genuine scores and 527875 imposter scores in the IITD database. The verification error rates FAR, FRR are calculated for the different thresholds and ROCs are plotted. These results are compared with the state of the art method, competitive coding scheme [35].

Tables 4.15-4.17 give EER and GAR for the lowest FAR for all the three databases. In terms of EER, the proposed method outperforms the competitive coding scheme for the three databases. Genuine acceptance rates at the lowest false acceptance rates (FAR) for the IITD and the GPDS databases are better than those of the competitive coding scheme. But, GAR for the PolyU database is 5% less than that of competitive coding scheme. All the ROCs for different lengths of PCCs for all the databases are given in the Figs. 4.1.2-4.1.4. Even though the results on the PolyU database are not better than those of the competitive coding scheme, EER and GAR are still acceptable. These figures show that the proposed method for palmprint verification provides a consistent performance.

Table 4.15: EERs and GARs of [35] and proposed method for different lengths of PCCs on the PolyU database.

Method	EER	GAR @ Lowest FAR
Competitive Code	0.30	97.89
PCC 3040	0.26	92.60
PCC 3188	0.33	89.20
PCC 2740	0.32	89.90
PCC 2752	0.42	89.80

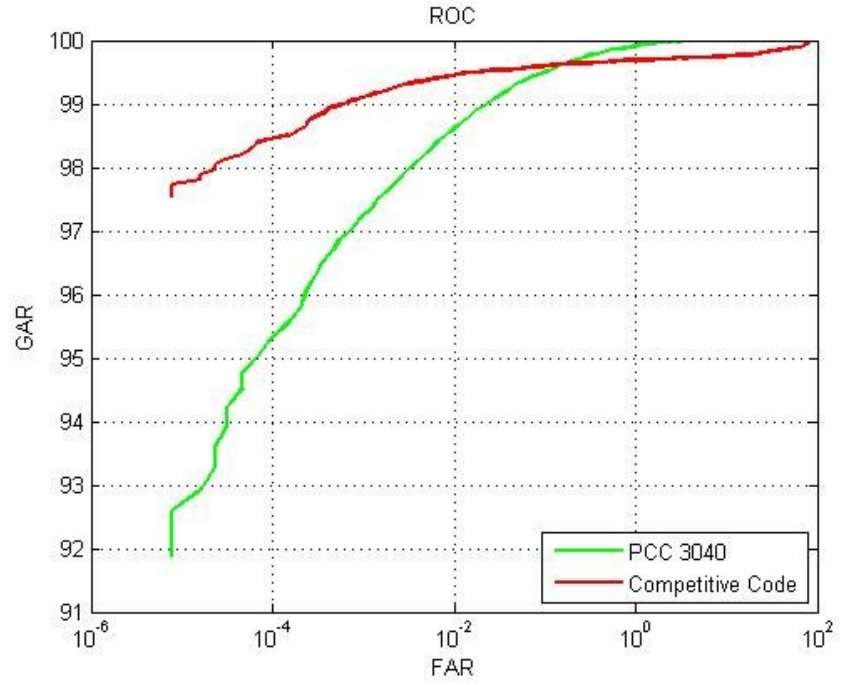

(a)

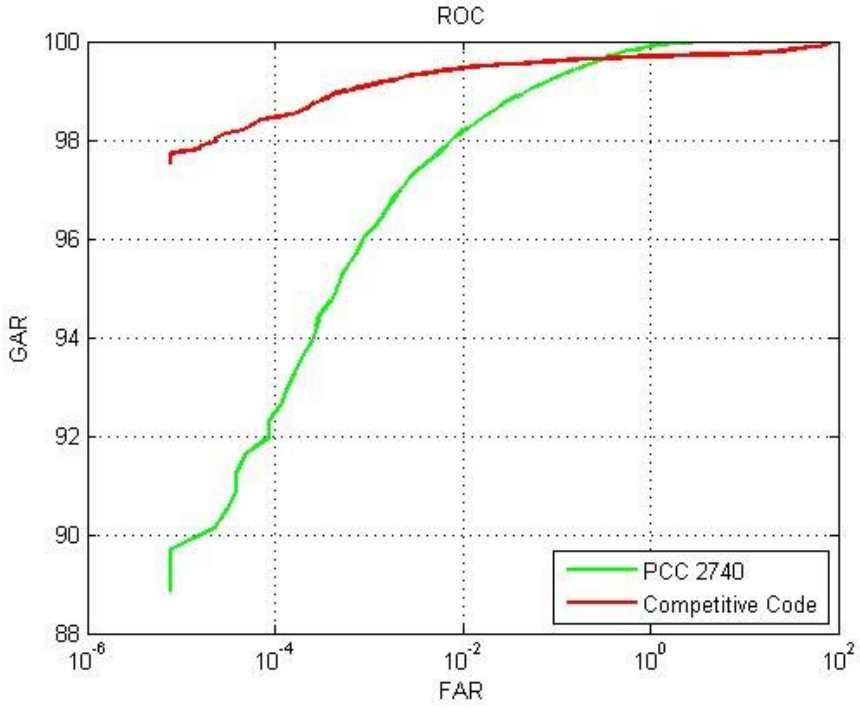

(b)

Figure 4.2: Comparisons of ROCs of the PolyU database for proposed method and competitive coding scheme [35], (a) 3040-bit PCC vs. [35], (b) 2740-bit PCC vs. [35].

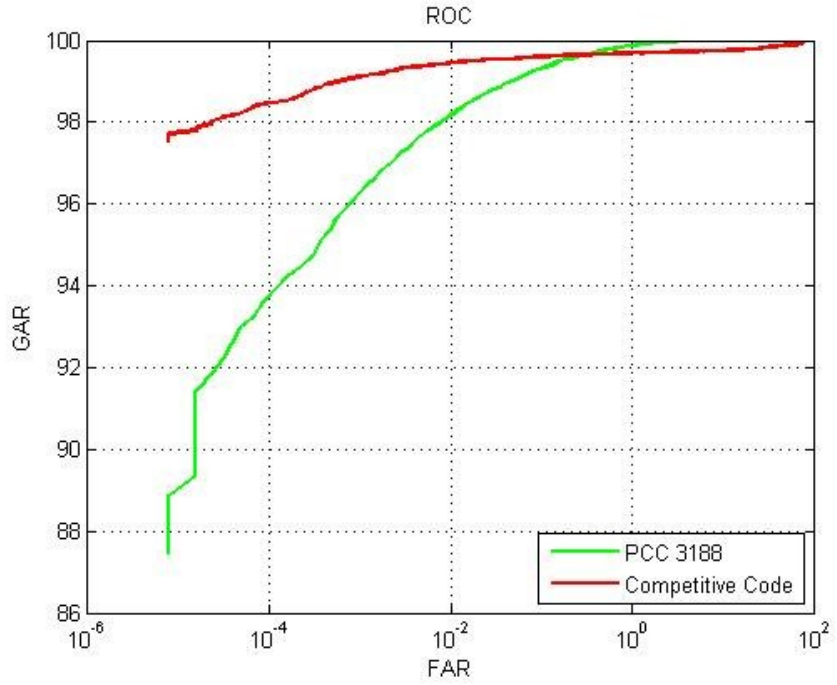

(a)

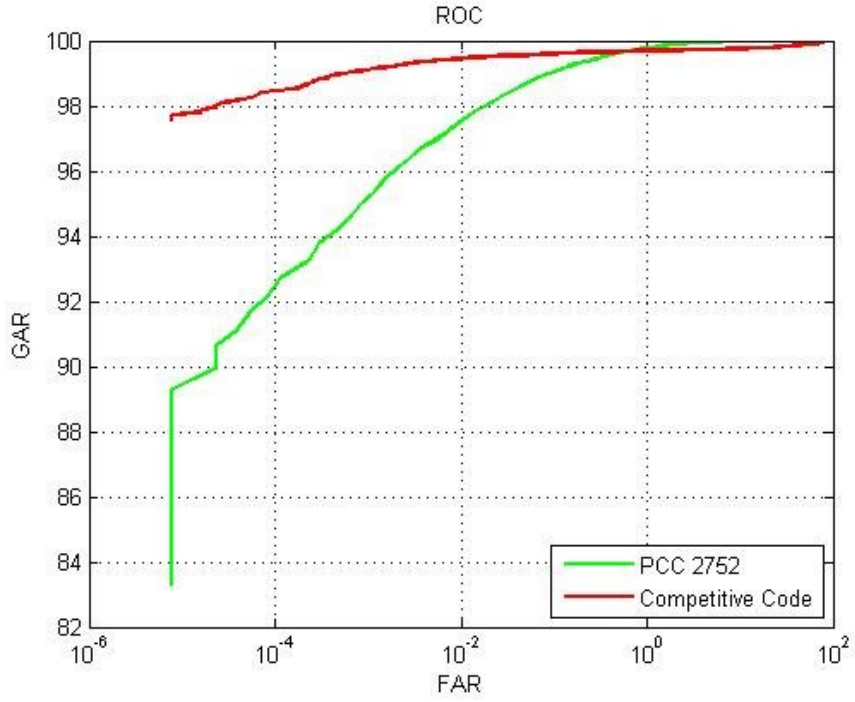

(b)

Figure 4.3: Comparisons of ROCs of the PolyU database for proposed method and competitive coding scheme [35] (a) 3188-bit PCC vs. [35] and (b) 2752-bit PCC vs. [35].

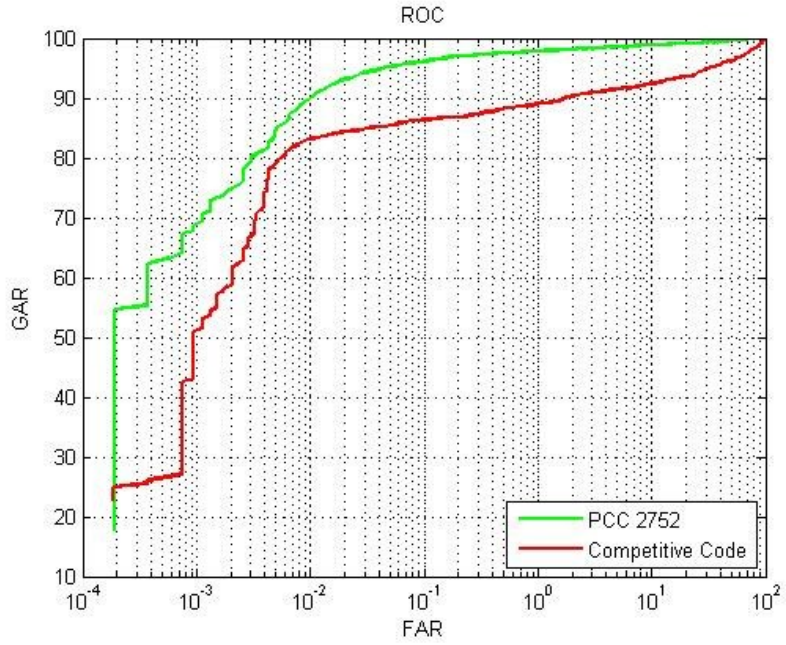

(a)

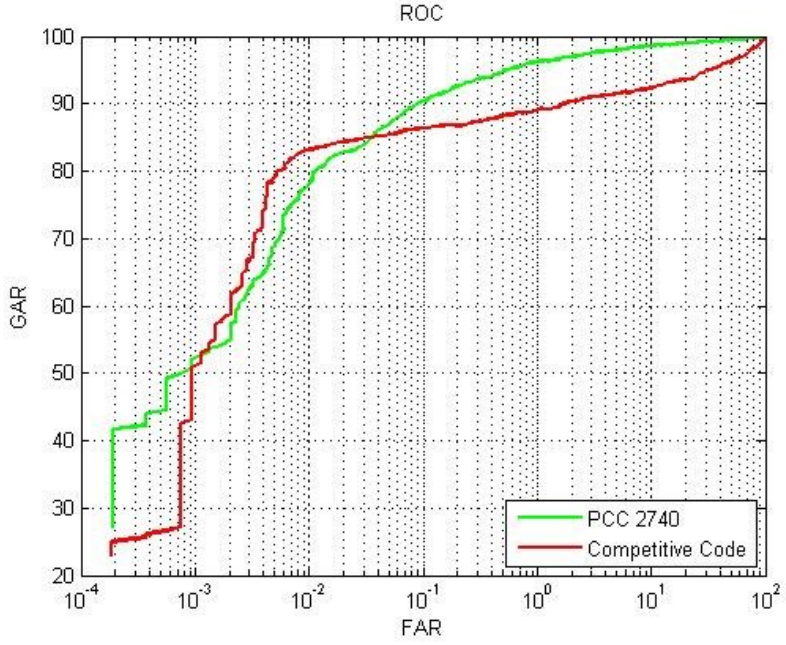

(b)

Figure 4.4: Comparisons of ROCs of the IITD database for proposed method and competitive coding scheme [35], (a) 2752-bit PCC vs. [35] and (b) 2740-bit PCC vs. [35].

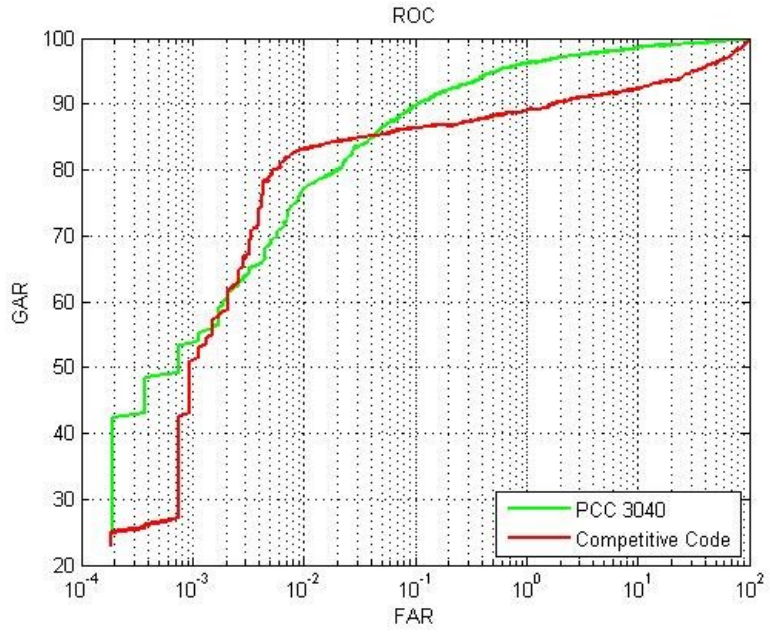

(a)

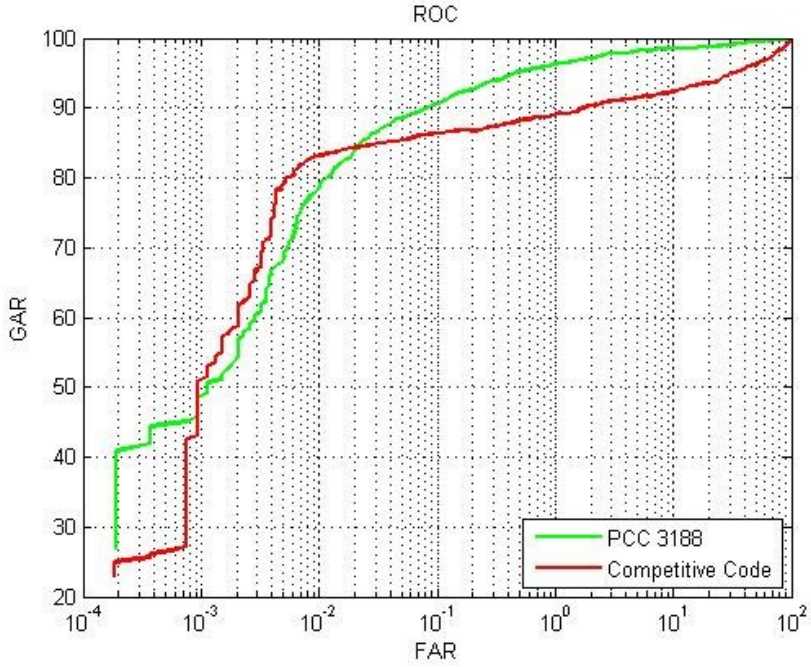

(b)

Figure 4.5: Comparisons of ROCs of the IITD database for proposed method and competitive coding scheme [35], (a) 3040-bit PCC vs. [35] and (b) 3188-bit PCC vs. [35].

Table 4.16: EERs and GARs of [35] and proposed method for different lengths of PCCs on the IITD database.

Method	EER	GAR @ Lowest FAR
Competitive Code	7.00	26.50
PCC 2752	1.87	54.80
PCC 2740	2.67	42.30
PCC 3040	2.64	43.50
PCC 3188	2.52	41.10

Table 4.17: EERs and GARs of [35] and proposed method for different lengths of PCCs on the GPDS database.

Method	EER	GAR @ Lowest FAR
Competitive Code	0.8636	90.80
PCC 2928	0.7329	89.30
PCC 2752	0.6322	92.50
PCC 3052	0.4750	88.00

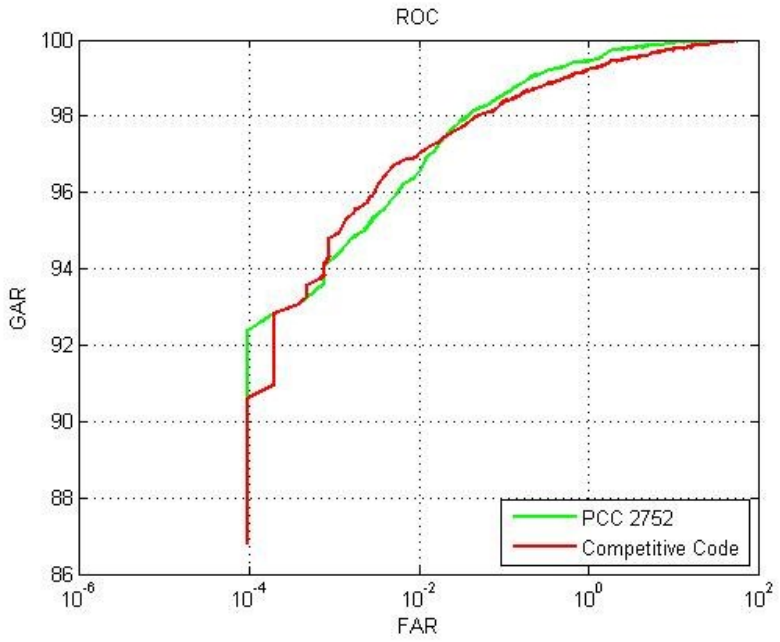

Figure 4.6: Comparison of ROCs of 2752-bit PCC and the competitive coding scheme [35] on the GPDS database.

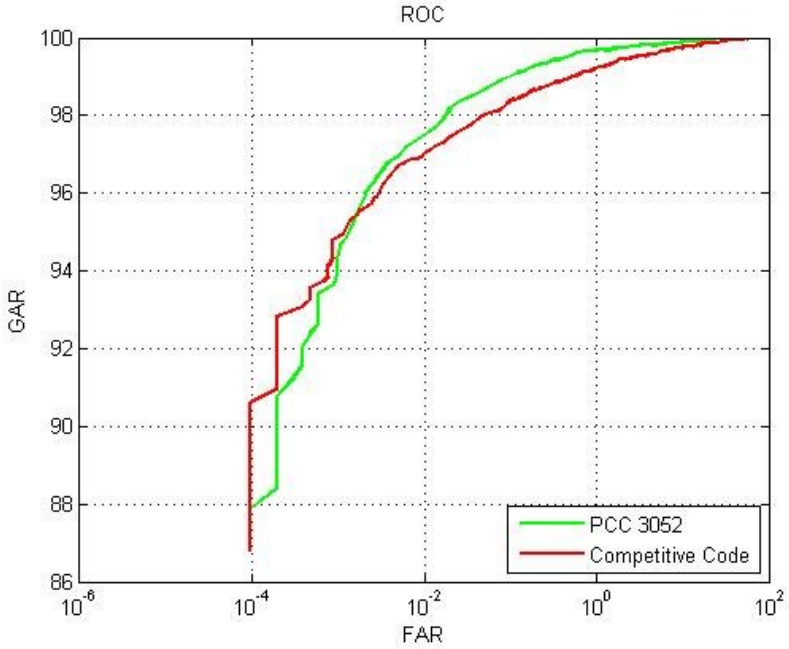

(a)

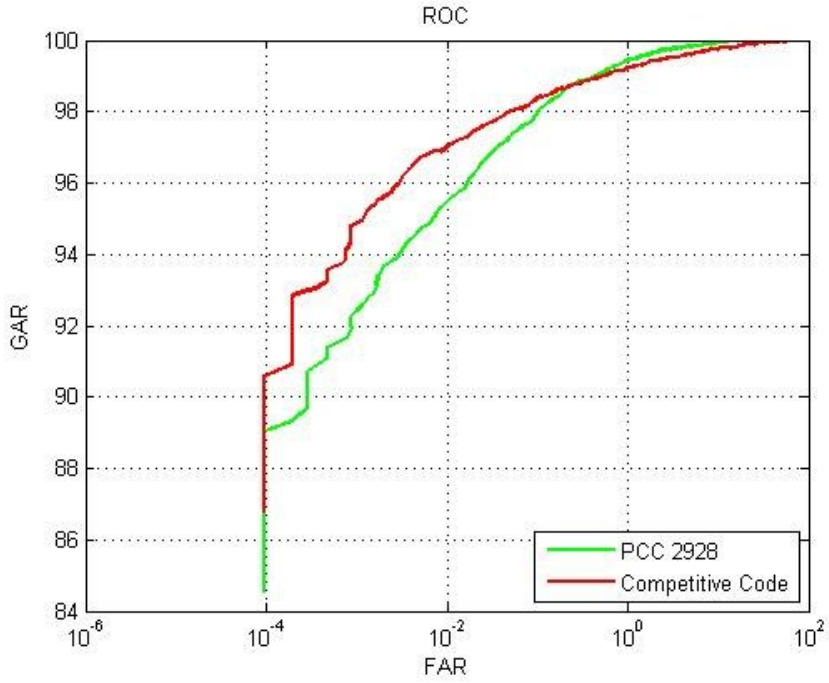

(b)

Figure 4.7: Comparisons of ROCs of the GPDS database for proposed method and competitive coding scheme [35], (a) 3052-bit PCC vs. [35] and (b) 2928-bit PCC vs. [35].

4.2 Experiments on Bi-modal System

In this section, experiments on bi-modal biometric system using fusion of face and palm at pixel level are detailed. In the proposed bi-modal biometric system two different biometric traits, namely, face and palm of the same person are required, but a bi-modal database is not available. Therefore, two different databases are selected, one for face and one for palm. A fixed pair of face and palm images are selected and formed a bi-modal database. The AT & T face database and the PolyU palm database are selected for the experiments. These databases are explained in Section 2.5. The AT & T database [19] consists of 400 images from 40 different persons, with 10 samples for each person. The PolyU database [17] contains 7752 images of 386 different palms, with 20 samples for each palm. To match the size, images of the entire AT & T database are selected and 400 palm images from the PolyU palm database are selected. As discussed in Section 2.5, the PolyU palm images have been collected in two different sessions, ten samples in each session. Therefore, for this fusion experiments, the first 40 classes of the palm database are selected, and for each class, first 5 samples from session one and last 5 samples from session 2 are selected to complete 10 samples set.

Palm images are enhanced as discussed in Section 3.2.1. A 3 x 3 Gaussian lowpass filter with standard deviation of 0.5 is applied to smooth the palm image and adaptive histogram equalization is applied to enhance the palm images. Since the fusion process requires same size images of face and palm, the processed palm images of size 128 x 128 are resized to the size of the face image (112 x 92) using bicubic interpolation [39].

Both the images are decomposed into 3 scales. Scale 1 of the curvelet transform is a low pass image whereas scale 2 and scale 3 are the bandpass images. Scale 2 bandpass image is decomposed into 8 directional bandpass images and scale 3 into 16 directional bandpass images. The *mean-mean fusion* rule as explained in Section 3.2 is used for the fusion. Two experiments are conducted to test the proposed method.

In first experiment, the performance of the method is verified against the number of training samples. Since performance with small sample size is the main objective, number of training samples (N_{TS}) is limited to 1, 2, and 3. The average identification rates are calculated for each experiment. Experiments are repeated for all the possible training sample sets. Since both the sessions of the PolyU palm images are used in the fused database, samples are taken only from session one. Out of 10 samples 5 are from session 1 and the remaining are from session 2. If the number of training samples is 2, then 2 images can be selected in 20 ways from 5 samples. Experiments are repeated for all these 20 possibilities; similarly there are 20 possibilities if the number of training samples is 3. For all these experiments number of PCA components (N_{PCA}) is fixed to the maximum. Table 4.18 gives the identification results when the number of training samples (N_{TS}) is 1. These results are the average of 10 experiments. The threshold values are obtained empirically. Three sets of training samples are taken to calculate the maximum distance of the registration database from the test database. The average value of these three distances is selected as a threshold. Same training sets are used for face, palm and fused databases. From Table 4.18, it is clear that even with single sample registration database, the proposed method achieves above 90% identification rates

and the deviation from the average CIR is less than those of face and palm. The recognition rates for training samples 2 and 3 are given in tables 4.19 and 4.20. The best and the worst recognition rates for different sizes of training sets are given in the Tables 4.21-4.23. It can be seen from these tables that even the worst case recognition rates of the proposed method are better than those of the eigenfaces and eigenpalms. The proposed method outperforms eigenface [29] and eigenpalm techniques and yields best recognition rates with small sample training sets.

In second experiment, the performance of the proposed method is evaluated in terms of the number of PCA components. Number of PCA components decides the feature vector dimension. Experiments are conducted for all the possible training samples and the average identification rates are presented. The recognition rates vs. number of PCA components for training samples 1, 2, and 3 are shown in Figs. 4.2.1-4.2.3, respectively. From these figures it can be observed that the proposed method yields almost 7 to 10% improvement compared to eigenfaces [29].

In the third experiment, the performances of the wavelet fusion and the curvelet fusion are compared. Face and palm images are fused using Haar wavelet, decomposing to 3 scales. The experiments are repeated for all the possible training sets. All the recognition rates for all the possible cases are plotted for both the fusion schemes in Fig. 4.2.3-4.2.5. From these figures it can be seen that, in most of the cases the curvelet fusion is better than the wavelet fusion.

4.3 Summary

In this chapter, comprehensive set of experiments have been conducted on three palmprint databases to evaluate the performance of the proposed PCC. The performance of the PCC has been verified on two modes of palmprint based biometric systems namely identification mode and verification mode. It has also been demonstrated that the proposed PCC can be used in hierarchical identification. The extensive experiments and the results indicate that the proposed PCC is a better choice compared to other existing methods. Extensive experimentation in terms of feature vector dimensions and number of training samples have been conducted on proposed pixel-level fusion method and showed that proposed fusion method yields better recognition rates compared to eigenfaces [29] and eigenpalms.

Table 4.18: Performance evaluation of fusion method for N_{TS} = 1, N_{PCA}= 40, and N_{TE} = 10.

Biometric System	Mean CIR (%) ± Deviation	Mean FIR (%)	Mean FRR (%)	Threshold (x 10^3)
Palm	82.02 ± 1.72	17.5	0.47	1.161
Face	69.77 ± 2.77	29.88	0.33	1.142
Proposed	90.47 ± 1.10	8.58	0.94	0.834

Table 4.19: Performance evaluation of fusion method for N_{TS} = 2, N_{PCA}= 80, and N_{TE} = 20.

Biometric System	Mean CIR (%) ± Deviation	Mean FIR (%)	Mean FRR (%)	Threshold (x 10^3)
Palm	85.64 ± 1.83	12.53	1.82	1.158
Face	81.17 ± 2.43	18.29	0.53	1.14
Proposed	91.76± 1.53	3.10	5.12	0.805

Table 4.20: Performance evaluation of fusion method for N_{TS} = 3, N_{PCA}= 120, and N_{TE} = 20.

Biometric System	Mean CIR (%) ± Deviation	Mean FIR (%)	Mean FRR (%)	Threshold (x 10^3)
Palm	86.01 ± 2.27	10.32	3.66	1.172
Face	86.87 ± 2.23	12.64	0.48	1.13
Proposed	93.66 ± 1.38	3.44	2.89	0.839

Table 4.21: The best and the worst CIRs of eigenface, eigenpalm, and the proposed fusion method with number of training samples = 1.

Biometric System	CIR	
	The Best CIR	The Worst CIR
Palm	84.16	78.88
Face	72.50	64.72
Proposed	92.77	89.16

Table 4.22: The best and the worst CIRs of eigenface, eigenpalm, and the proposed fusion with number of training samples = 2.

Biometric System	CIR	
	The Best CIR	The Worst CIR
Palm	89.68	82.81
Face	85.62	77.50
Proposed	95.31	89.06

Table 4.23: The best and the worst CIRs of eigenface, eigenpalm, and the proposed fusion method with number of training samples = 3.

Biometric System	CIR	
	The Best CIR	The Worst CIR
Palm	90.35	82.50
Face	91.07	83.92
Proposed	96.78	90.35

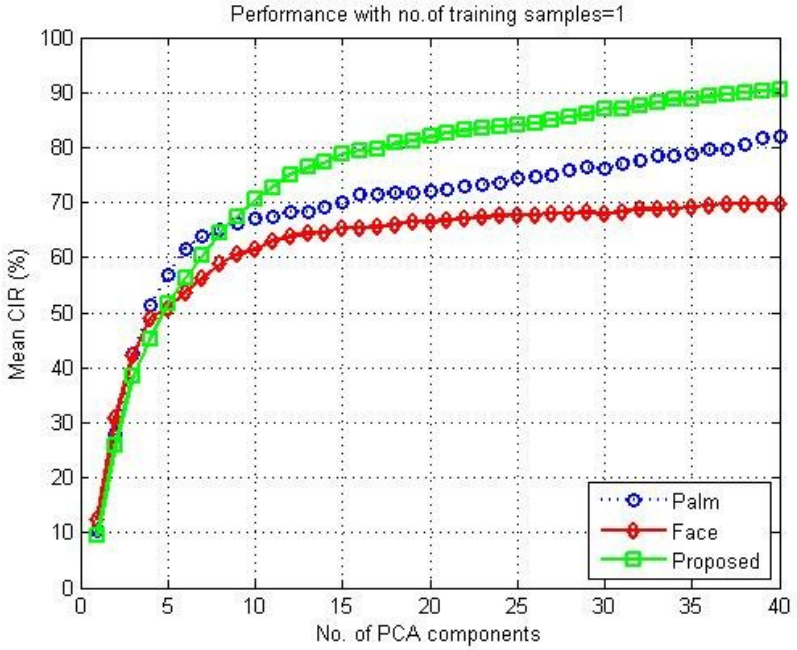

Figure 4.8: Recognition rates of the three methods against varying N_{PCA}, when N_{TS} = 1.

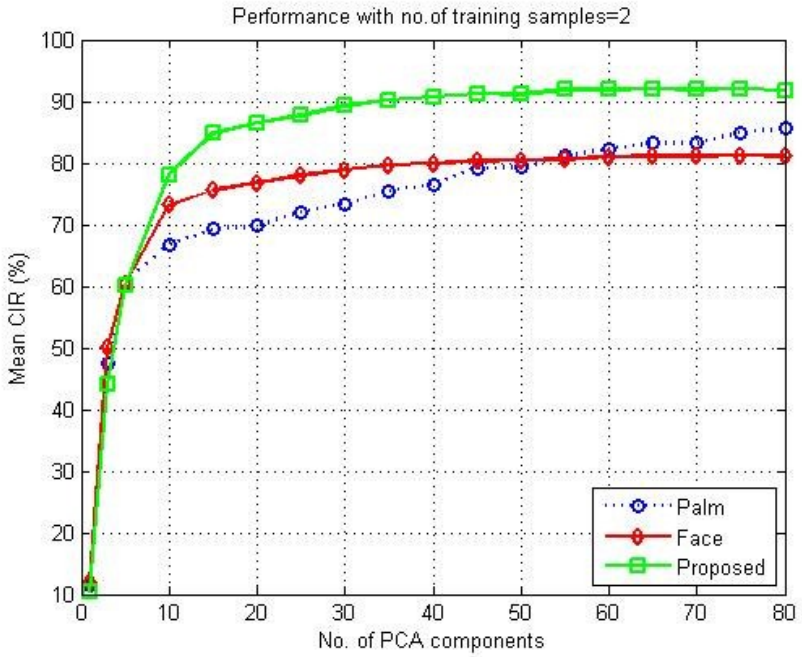

Figure 4.9: Recognition rates of the three methods against varying N_{PCA}, when N_{TS} = 2.

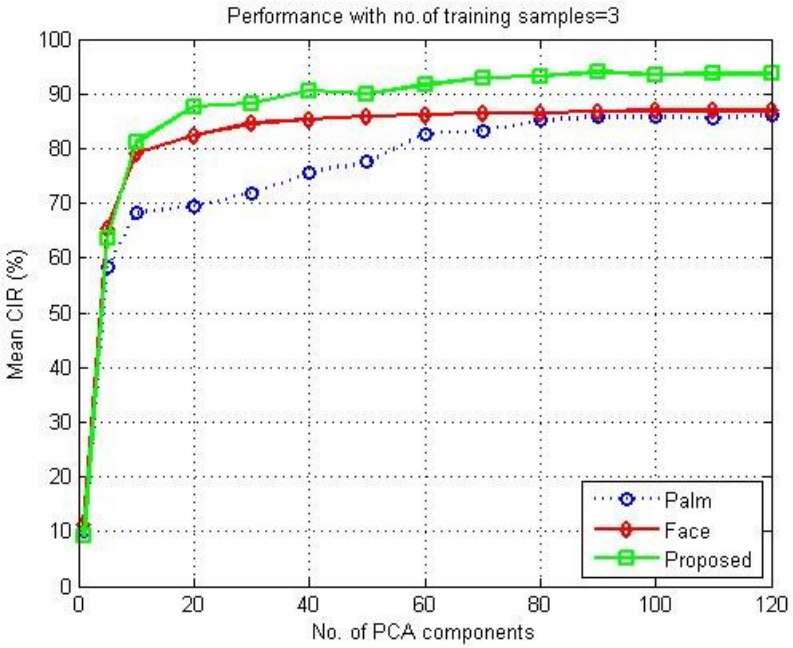

Figure 4.10: Recognition rates of the three methods against varying N_{PCA}, when N_{TS} = 3.

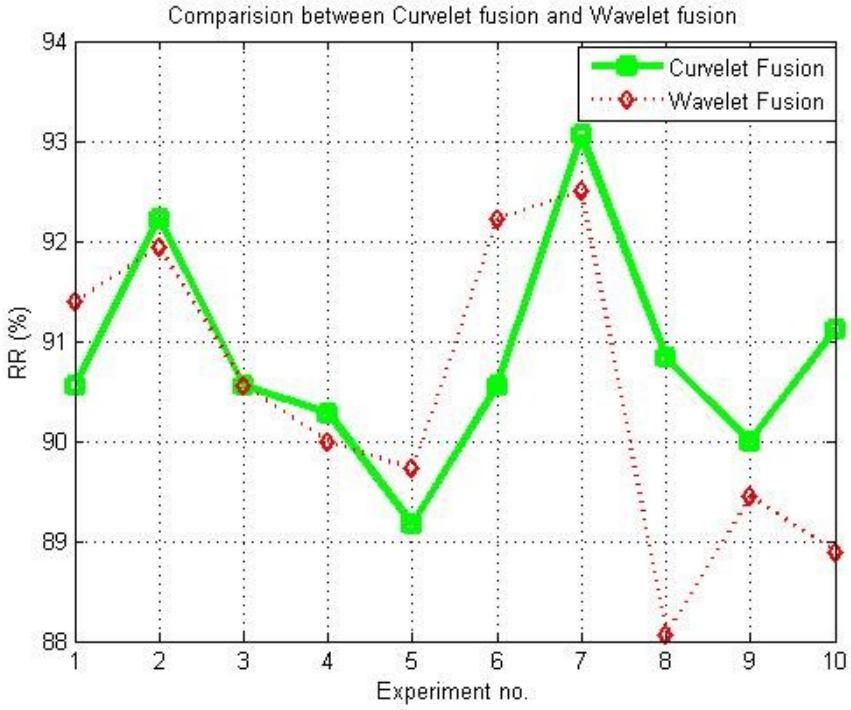

Figure 4.11: Comparison of the Wavelet fusion and the curvelet fusion for N_{TS} = 1.

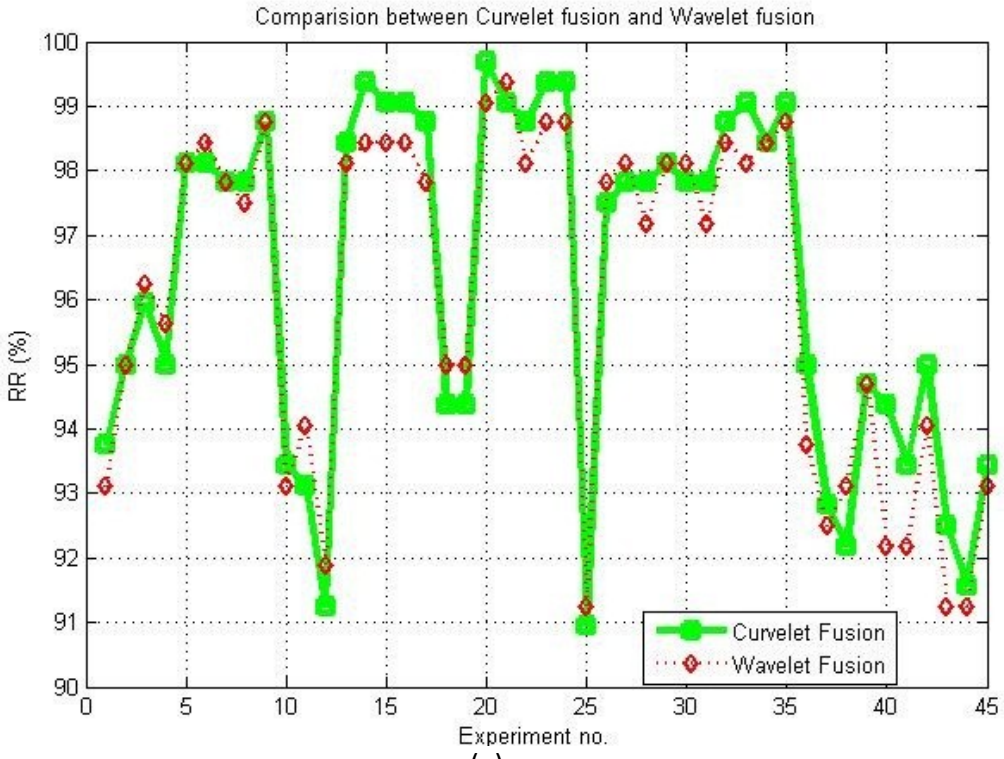

(a)

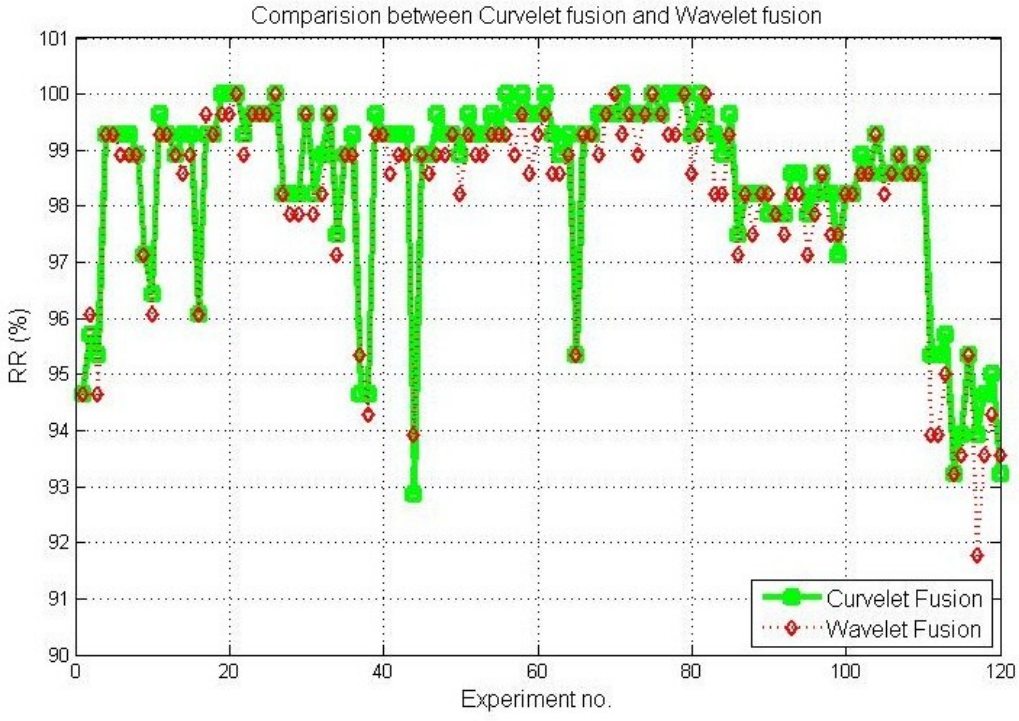

(b)

Figure 4.12: Comparisons of the Wavelet fusion and the Curvelet fusion for (a) N_{TS} = 2 and (b) N_{TS} = 3.

Chapter 5

Conclusion and Scope for Future Work

5.1 Concluding Remarks

Automatic person identification is an important task in our day-to-day life. Traditional identification methods are based on a claimed identity like personal identification number (PIN) and identity card. A disadvantage of these traditional identification methods is that any person with the claimed identity will be given authorization. The identity cards can be stolen and the PIN can be guessed. Therefore, it is desirable to identify the person based on "who he/she is?". Biometric person identification is a solution to this problem, in which the person is identified based on his/her physical or behavioral traits. Palmprint is one of the physical traits that can be used in online identification systems. The characteristics in a palmprint are in the form thick and thin lines called principal lines and wrinkles, respectively. As the lines and curves are scattered and have different thickness, a multi-scale and multi-directional representation is more appropriate to represent these principal lines and scattered wrinkles. Moreover this multi-scale and multi-directional representation is useful in image fusion. Curvelet transform is a multi-scale and multi-directional geometric

transform that requires relatively a small number of coefficients to represent edges and curves.

In this thesis, these desirable characteristics of the curvelet transform have been used to represent a palm image and two methods have been proposed to devise uni-modal and bi-modal biometric systems, respectively. In first method, a simple binary coding scheme has been used to represent the multi-scale and multi-directional structural information of palm images and a palm curvelet code (PCC) is obtained. In the second method, a pixel-level fusion scheme in the curvelet domain has been used for a face and palm based bi-modal biometric system.

The performances of both the uni-modal and bi-modal biometric systems have been evaluated using extensive experimentation. The performance of PCC has been evaluated on three publicly available palm databases, namely, PolyU, GPDS, and IITD. It has been shown that PCC yields higher identification rates and provides a consistent performance. It has also been shown how PCC can address the problem of identification in large databases and demonstrated that hierarchical identification using PCC improves the speed of matching at the cost of a very little loss in accuracy. The execution times for both in MATLAB and C++ have been presented and shown the feasibility of the method in real time applications. The performance of the fusion method for a bi-modal biometric system has been evaluated on AT&T face database and PolyU palm database. Palm and face images have been fused in the curvelet transform domain using *mean-mean fusion* rule and a subspace method, principal component analysis (PCA), has been

used in feature extraction and matching of the fused images. Performance evaluation of the proposed fusion method in terms of the size of the training samples and the recognition rates has shown to provide a better performance compared to that of eigenfaces and eigenpalms.

5.2 Scope for Future Work

The work in this thesis can be modified in a number of ways to improve the speed and performance. The following is a brief description of possible areas of future investigation.

- In palm verification using PCC, the palm images are translated in 8 directions to avoid translational errors. The effect of translation in curvelet directional bands may be studied and different translated PCCs from the curvelet transform of a single image may be obtained. This process should improve the speed in the verification process.
- An optimized set of directional bandpass images may be selected to generate a PCC. All the directional bandpass images of a particular palm may not be useful in identifying the palm from a database. There may be a set of bandpass images having large deviation from the imposters. For each palm image in the database, one could select a set that is most optimized. This set can be obtained by training images. Optimization algorithms such as particle swarm optimization (PSO) [40] may be used to find an optimum set for a particular palm class. The algorithm should target to improve some of the performance evaluation parameters, such

as EER and the area under the curve of ROC. With an optimized set of directional bandpass images, variable length PCCs may be generated. This process may improve the accuracy and the speed of identification.

- The idea of optimization may also be applied to the fusion based bi-modal biometric system. Fusion may be carried out for a selected number of sub-bands to improve the accuracy. Other feature extraction and classification methods, such as independent component analysis (ICA) and Fisher linear discriminant analysis (FLDA) may be studied.

References

[1] D. Zhang, *Palmprint Authentication*, Kluwer Academic Publishers, USA, 2004.

[2] Adams Kong, David Zhang, and Mohamed Kamel, "A survey of palmprint recognition", *Pattern Recognition*, vol. 42, pp. 1408-1418, 2009.

[3] Xiang-Qian Wu, Kuan-Quan Wang, and David Zhang, "Wavelet based palmprint recognition", in *Proc. First Int. Conf. Machine learning and Cybernetics,* Beijing, pp. 153-1257, 2002.

[4] Lei. Zhang and Zhang D, "Characterization of palmprints by wavelet signatures via directional context modeling", *IEEE Trans. Systems, Man and Cybernetics-Part B*, vol. 34, pp. 1335-1347, 2004.

[5] Zhang, D.; Wai-Kin Kong; You, J.; Wong, M.; "Online Palmprint Identification", *IEEE Trans. Pattern Analysis and Machine Intelligence*, vol. 25, pp. 1041-1050, 2003.

[6] Chen, G.Y.; Bui, T.D.; Krzyzak, A.; "Palmprint classification using dual-tree complex wavelets", *IEEE Int. Conf. on Image Processing*, Atlanta, GA, 2006, pp. 2645-2648.

[7] Chen, G.Y.; and Kegl, B.; “Palmprint classification using contourlets”, *IEEE Int. Conf. on Systems, Man and Cybernetics*, Montreal, 2007, pp. 1003-1007.

[8] Kaifeng Dong, Guiyu Feng, and Dewen Hu, “Digital curvelet transform for palmprint recognition”, *Sinobiometrics*, S.Z. Li et al. Eds., LNCS 3338, pp. 639-645, 2004.

[9] Lei Zhang, Zhenhua Guo, Zhou Wang, and David Zhang, “Palmprint verification using complex wavelet transform”, *IEEE Int. Conf. on Image Processing*, San Antonio, pp. II - 417 - II - 420, 2007.

[10] Fang Li, Leung, M.K.H, and Xiaozhou Yu, “Palmprint identification using Hausdorff distance”, *IEEE workshop on Biomedical Circuits and Systems*, pp. s3/3-s5/8, 2004.

[11] Tee Connie, Andrew Teoh Beng Jin, Michael Goh Kah Ong, and David Ngo Chek Ling, “An automated palmprint recognition system”, *Image and Vision Computing*, vol. 23, pp. 501-515, 2005.

[12] Chin-Chuan Han, Hsu-Liang Cheng, Chih-Lung Lin, and Kuo-Chin Fan, “Personal authentication using palm-print features”, *Pattern Recognition*, vol. 36, pp. 371-381, 2003.

[13] Emmanuel Cand`es, Laurent Demanet, David Donoho, and Lexing Ying, “Fast Discrete Curvelet Transforms”, available at http://www.curvelet.org/papers/FDCT.pdf

[14] Jainwei Ma and Plonka, G., "The Curvelet Transform", *IEEE Signal Processing Mag.*, vol. 27, pp. 118-133, 2010.

[15] Ajay Kumar, "Incorporating Cohort Information for Reliable Palmprint Authentication," in *Proc. 6th Indian Conf. Vision, Graphics and Image Proc.(ICVGIP)*, Bhubneshwar, India, pp. 583-590, Dec. 2008.

[16] IIT Delhi palmprint image database version 1.0, available at http://web.iitd.ac.in/~ajaykr/Database_Palm.htm

[17] PolyU palmprint database, available at http://www.comp.polyu.edu.hk/~biometrics

[18] Miguel A. Ferrer, Aythami Morales, Carlos M. Travis o and Jesús B. Alonso, "Low Cost Multimodal Biometric Identification System based on Hand Geometry, Palm and Finger Textures", in *41st Annual IEEE International Carnahan Conference on Security Technology*, ISBN: 1-4244-1129-7,pp. 52-58, Ottawa, Canada, 8-11 October 2007.

[19] AT & T face database, available at http://www.cl.cam.ac.uk/research/dtg/attarchive/facedatabase.html

[20] Ishrat Jahan Sumana, "*Image retrieval using discrete curvelet transform*", A master's thesis from Monash University, Australia, available at, http://personal.gscit.monash.edu.au/~dengs/resource/papers/Sumana_Thesis.pdf

[21] Sumana, I.J.; Islam, M.M.; Dengsheng Zhang; Guojun Lu,"Content based

image retrieval using curvelet transform", *IEEE 10th workshop on Multimedia and Signal processing*, Cairns, Qld., pp.11-16, 2008.

[22] Ajay Kumar, David C. M. Wong, Helen C. Shen, and Anil K. Jain, "Person verification using palmprint and hand geometry biometric", *Audio and video based biometric person authentication*, J. Kittler and M. S. Nixon Eds., LNCS 2688, pp. 668-678, 2003.

[23] Atif Bin Mansoor, M.Mumtaz, H.Masood, M.Asif A. Butt, and Shoab A. Khan, "Person identification using palmprint and contourlet transform", *Advances in Visual computing*, G Bebis et al. Eds., LNCS 5359, pp. 521-530, 2008.

[24] C. Sanderson and K.K. Paliwal, "Information fusion and person verification using speech and face information", Research Paper IDIAP-RR 02-33, IDIAP, September 2002.

[25] Anil Jain, Kathik nandakumar, and Arun Ross, "Score Normalization in Multimodal Biometric Systems", *Pattern Recognition*, vol. 38, pp. 2270-2285, 2005.

[26] Xiao-Yuan Jing, Yong-Fang Yao, David Zhand, Jing-Yu Yang, and Miao Li, "Face and palmprint pixel level fusion and Kernel DCV-RBF classifier for small sample biometric recognition", *Pattern Recognition*, vol.40, issue 11, , pp. 3209-3224, 2007.

[27] Kisku, D.R.; Rattani, A.; Gupta, P.; and Sing, J.K.; , "Biometric Sensor Image

Fusion for Identity Verification: A Case Study with Wavelet-based Fusion Rules and Graph Matching", *IEEE Conf. Technologies for Homeland security*, Boston, MA, pp.433-439, 2009.

[28] Curvelets tool box, available at: http://www.curvelet.org.

[29] M. Turk and A. Pentland, "Face Recognition using Eigenfaces", *Proc. Computer Vision and Pattern Recognition*, pp 586-591, 1991.

[30] Bin Zhang and Sargur N. Srihari, "Properties of binary vector dissimilarity measures", available at http://www.cedar.buffalo.edu/papers/articles/CVPRIP03_propbina.pdf

[31] Official web-site. Available: http://en.wikipedia.org/wiki/Principal_component_analysis

[32] M.S. Bartlett, J.R. Movellan and T.J. Sejnowski, Face Recognition by Independent Component Analysis, *IEEE Trans. on Neural Networks*, vol. 13, No. 6, pp. 1450-1464, November 2002.

[33] Ekinci .M and Aykut, M. "Gabor-based kernel PCA for palmprint recognition", *Electronic letters*, vol. 43, pp. 1077-1079, 2007.

[34] Wu, X., Zhang, D., and Wang, K., "Fisher palms based palmprint recognition", *Pattern Recognition. Letters,* 2003, 24, (15), pp. 2829–2838.

[35] Adams Kong and David Zhang, "Competitive Coding scheme For Palmprint Verification", *IEEE 17th Int. Conf. Pattern Recognition*, vol. 1, pp. 520-523, 2004.

[36] Official web-site. Available: http://opencv.willowgarage.com/wiki/

[37] Official web-site. Available: http://mplab.ucsd.edu/~marni/code.html

[38] Yoav Freund and Robert E. Schapire, "A decision-theoretic generalization ofon-line learning and an application to boosting," *Journal of Computer and System Sciences*, vol. 55, no. 1, pp. 119-139, 1997.

[39] Rafael C. González and Richard Eugene Woods, "*Digital Image Processing*", 3rd ed., Prentice Hall, 2008.

[40] Kennedy, J.; Eberhart, R.;, "Particle swarm optimization", in *Proc. IEEE Int. Conf. on Neural networks*, Perth, pp. 1942-1948, 1995.

[41] Anil K. Jain, Ruud Bolle, and Sharath Panakanti, *Biometrics: personal identification in networked society*, Kluwer Academic Publishers, USA, 2004.